Testing, numerical modelling and design of Q690 high-strength steel welded T-section stub columns

Jun-zhi Liu[1]; Shuxian Chen[1]; Tak-Ming Chan[1,2] *

[1] Department of Civil and Environmental Engineering, The Hong Kong Polytechnic University, Hong Kong, China

[2] Chinese National Engineering Research Centre for Steel Construction (Hong Kong Branch), The Hong Kong Polytechnic University, Hong Kong, China

* Corresponding author: tak-ming.chan@polyu.edu.hk

Abstract

This paper presents a comprehensive experimental and numerical investigation into the material properties and stub column behaviour of Q690 high-strength steel (HSS) welded T-sections. A total of 16 concentrically loaded stub column tests were performed. The Q690 HSS welded T-sections were fabricated from 6 mm and 10 mm thick plates, delivered in quenched and tempered (QT) conditions by means of gas metal arc welding (GMAW). Material properties measurements were carried out on the coupon specimens taken from the parent plates. Initial local geometric imperfection measurements were conducted. In conjunction with experimental tests, finite element (FE) models were developed to replicate the test results and failure modes. Afterwards, the validated FE models were adopted to conduct parametric studies to supplement the experimental data by generating further structural performance data covering a broader range of cross-section slenderness. Cross-section slenderness limits set out in design codes such as EN 1993-1-12, ANSI/AISC 360-16, AS 4100 and design methods of DSM as well as CSM were evaluated against the experimental and numerical data. It was found that the current limits are generally accurate and safe in three design codes and the cross-section slenderness of DSM is accurate and comparably conservative. Cross-section capacities predictions obtained from EN 1993-1-12, ANSI/AISC 360-16, AS 4100, DSM and CSM were also compared with the tests and numerical results. It is shown that the established local buckling design provisions in EN 1993-1-12 and ANSI/AISC 360-16 result in more precise and consistent predictions compared with AS 4100, DSM and CSM.

Keywords: Stub column tests; Finite element modelling; Local buckling behaviour; High strength steel; Design analysis

1. Introduction

The advancement in material industries and manufacturing techniques facilitate the application of high-strength steel (HSS) civil engineering structures. HSS with nominal yield strength higher than 460 MPa possess advantageous mechanical properties such as high strength-to-weight ratios, resulting in the reduced dimensions of the structural components. This makes HSS a competitive and prospective material particularly for large-span and high-rise civil engineering structures [1, 2]. Experimental and numerical investigations have been previously conducted on various types of cross sections with different fabrication methods. A brief summary of the experimental studies is introduced herein. In past years, local buckling behaviour of HSS welded sections fabricated by welding HSS A514 plates (nominal yield strength = 690 MPa) have been carried out by Nishino et al. [3] and Nishino and Tall [4]. Rasmussen and Hancock [5] carried out experimental investigation to study the local buckling performance for welded box sections comprising parent steel plates of BISALLOY 80 (nominal yield strength = 690 MPa). High-strength steel welded box sections fabricated by Q460 steel plates (nominal yield strength =460 MPa) was investigated by Shi et al. [6]. Schillo and Feldmann [7] reported experimental investigations on HSS welded box sections with strength grade of steel S500 and S960. Recently, HSS welded I-sections have been extensively investigated on cross-section behviours in [2, 8] with steel grade of S690 and S960, by which cross-section classification and cross-section strength predictions were compared with design codes. Moreover, flexure behaviour of the HSS welded I-sections was studied in [9, 10] at cross-section level. Particularly, the HSS welded-sections investigations in [10] examined hybrid sections with flange strength varying from yield strength of 355 MPa to 690 MPa. Following the technology advancement, investigation on local buckling behaviour and cross-section resistance have also been conducted on cold-formed HSS tubular sections including square hollow sections (SHSs), rectangular hollow sections (RHSs) and circular sections (CHSs) [11] as well as hot-finished sections of SHSs and RHSs [12-14]. The cross-section classification stipulated in the structural steel design codes and the strength predictions were evaluated and compared.

Based on the brief review on the investigations for HSS, the extensive experimental studies have been performed for high-strength steel with doubly-symmetric section such as the welded sections of box-section, I-section as well as the cold-formed sections of CHS, SHS, RHS whereas the investigation on their non-doubly counterpart sections remained fairly limited. Compared with the doubly-symmetric tubular or open cross sections, non-doubly symmetric cross sections are relatively simpler to be fabricated with reduced manufacturing costs but are more prone to instability associated buckling problems, particularly torsion related buckling. Moreover, non-doubly symmetric cross-sections have great flexibility to suit the structural configurations. Though non-doubly symmetric sections exhibit rather simple cross-section shapes, buckling behaviour and the strength design are rather complicated. The applicability of the design codes and the design methods for doubly-symmetic sections need to be re-assessed and evaluated for non-doubly symmetric sections. The experimental investigations for angle section and channel sections have been studied by Zhang et al. [1] and Wang et al. [15] with nominal yield strength up to 690 MPa and 960 MPa. Cao et al. [16] conducted experimental and numerical analysis on HSS T-section columns with nominal yield strength up to 800 MPa. However, no research has been performed to study the cross-section behaviour of HSS welded T-section stub columns. T-section structural members can be found in purlins of roof truss structures as well as braces in offshore lattice tower structures. Thorough understanding its structural performance will facilitate the application of the HSS structural members comprising T-section members. Moreover, the current structural steel design specifications such as EN 1993-1-12 [17] generally stem from the conventional-strength steel regulations set out in EN 1993-1-1 [18] as a simple extension, which may not be applicable to the HSS T-section stub columns.

The aim of this paper is to investigate the cross-sectional behaviour and compression capacities of the HSS welded T-section stub columns experimentally and numerically. The experimental investigation was conducted on sixteen HSS T-section stub columns. The material properties were obtained through tensile coupon tests. Furthermore, initial local geometric imperfections measurements were carried out. After completion of the stub column tests, the obtained test results were employed to validate the developed finite-element (FE) model, by which the parametric studies were subsequently performed covering a wider spectrum of cross-section geometries. The generated experimental and numerical data were utilized to compare and assess the strength predictions and applicability of the current design provisions and formulae, specified in EN 1993-1-12 (CEN 2007) [17], North American specification ANSI/AISC-360-16 [18], Australian design code AS 4100 [19] as well as the developed design methods, Direct Strength Method (DSM) [20] and Continuous Strength Method (CSM) [21].

2. Test specimens

A total of 16 Q690 HSS welded T-section stub column specimens were tested. The HSS welded T-sections in this study were fabricated from the welded I-sections by wire-cutting, thus no heat treatment was involved and the thermal effect is minimized [22]. The HSS I-section was fabricated by welding three high-strength steel plates through gas metal arc welding (GMAW) with fillet welds. The selected electrode is in the category of ER110S-G with nominal yield strength 860 MPa and ultimate strength of 920 MPa, the detailed chemical compositions of electrode are presented in Table. 2. The high-strength steel plates Q690 are steel plates fabricated in accordance with the code of GB/T 1591-2018 [23], which were delivered in Quenched and Tempered (QT) condition with chemical compositions provided from manufacturer shown in Table. 1. The nominal thickness of the HSS plates was 6 mm and 10 mm respectively. Detailed definition of the symbols of the cross section are illustrated in Fig. 1, where H is the height of the cross section, B is the width of the flange, h_w is the clear width of the web, b_f is the clear width of the flange, h_f is the size of the fillet welding. A specimen designation system including detailed dimensions of the geometries of the cross section is utilized in the paper. The letter "T" is used to represent the T-shaped cross section, "SC" is used to indicate the stub column and nominal dimensions of $H \times t_w$ (in mm) following after the hyphen. For example, a label of "T-SC-100 × 6#" indicates a T-section specimen with nominal overall height of 100 mm, and the nominal thickness of the web is 6 mm, and the symbol "#" indicates that it is a repeated test specimen. The dimensions of the cross-section of the specimens were designed to cover a relatively larger spectrum of the b/t ratio varying between 5.7 and 31.1 (resulting in cross-section slenderness λ_p varying from 0.56 to 3.05). The measured dimensions of the specimens are summarized in Table. 3 using the nomenclatures illustrated in Fig.1. In addition, the welding related parameters are briefly introduced. Two welding passes were applied and the current was varied between 120 A and 130 A while the voltage was varied between 19 V and 21 V with welding speed taking as average of the recording time as 120 mm/min. The linear heat input energy is strictly controlled by monitoring the welding speed with linear heat input lower than 1.05 kJ/mm, as the high linear heat input necessarily induces negative impact on the material properties. The linear input energy can be determined in accordance with the expression shown in Eq. (1). The effect of the linear heat input on the material properties have been investigated in [24, 25] HSS materials. No reduction in terms of yield strength and ultimate strength for S700 steel plate with a linear heat input value less than 1.4 kJ/mm are concluded in [25] and only 2% decrease in yield strength and no reduction in ultimate strength were reported in [24] with a linear heat input value of 1.0 kJ/mm for S690-QT steel plate. Though heat affected zone were existed during the welding procedure, the impact of the linear heat input on the material properties in this study is negligible. Thus, in the further numerical analysis in section 6.2, the effect of welding on material properties is not explicitly accounted for.

$$Q = \frac{k \times U \times I \times 60}{v \times 1000} \tag{1}$$

where k is the thermal efficiency taken as 0.8 for GMAW [26, 27], U is the welding voltage in volt (V), I is the welding current in ampere (A), and v is the welding speed in millimeter per minute (mm/min).

3. Material properties

The material properties were determined based on tensile coupon tests. The tensile coupon specimens were machined from HSS parent plates with thicknesses of 6 mm and 10 mm. The tensile coupon specimens from the parent plates were extracted longitudinally and transversely. Three coupon specimens were taken in each direction for each thickness plate. Thus, twelve parent coupon specimens were taken from each parent plate. Instron 5982 testing machine, an electromechanical high force universal testing system with a capacity of 100 kN, was utilized to conduct the tensile coupon tests, as shown in Fig. 2. The dimensions of the coupon specimens were designed in accordance with ISO EN 6892-1: 2019 [28]. An optical non-contact video extensometer with gauge length of either 25 mm or 50 mm painted by the white dots was used to capture the full engineering stress-strain relationship up to fracture. The displacement control was applied with an initial loading speed 0.05mm/min up to the nominal yield strength and the loading speed was changed to 0.08 mm/min beyond nominal yield strength to speed up the process but maintain a low speed to mimic the static loading. Two strain gauges were adhered to the mid-height of the coupon specimens to measure the elastic modulus and the strain. The obtained stress-strain curves were employed to determine the yield strength and ultimate strength as well as other material properties. The measured properties of the parent plates are summarized in Tables. 4 – 5 for 6mm and 10 mm thick parent plates respectively, where E_s indicates the elastic modulus, f_y is yield strength, f_u is the ultimate strength, ε_{sh} is strain-hardening strain,

ε_u is strain at ultimate strength, ε_f, is elongation at fracture and ε_f is the proportional elongation at fracture. Typical stress-strain curves of the parent plates are plotted in Fig. 3 for 6 mm thick parent plates and Fig. 4 for 10 mm thick parent plates respectively.

4. Geometric imperfection

Initial local geometric imperfections were introduced into the HSS welded T-sections during the manufacturing process or transportation, which have great impact on the capacity resistance of the structures. The initial local imperfections were therefore measured for each HSS welded T-section stub column prior to the compressive testing. The set-up of the initial imperfection measurement such as the Linear Variable Displacement Transducers (LVDTs) arrangement of the measurement as well as the sign conventions of the measured local imperfection are depicted in Fig. 5. A milling machine was employed as a measurement platform on which the specimen was mounted. A set of three LVDTs with an accuracy of 0.001 mm was affixed to the head of the milling machine moving longitudinally along the length of the specimen to record the deviations. The same configurations of the imperfection measurements have been adopted by [11, 29]. Each surface of the specimens was measured with two LVDTs located near the sides and one at the mid portion of the constituent plate element. Measurement was taken at a 2 mm interval along the specimen length. For the purposes of eliminating the possible local imperfection caused by wire-cutting, the measurements were started and terminated at the location 20 mm away from each end of the specimen. The initial local geometric imperfection of the plate elements was taken to be the deviation between the measurement at the mid-portion and a straight datum line connecting the measurements at the sides. The measured maximum amplitudes (ω_0) of the local geometric imperfection for each specimen is reported in Table. 3. Fig. 6 depicts the typical measured initial local geometric imperfections profile along the web and flange of the T-section stub column.

5. Stub column tests

A total of 16 HSS welded T-section stub column tests were conducted to investigate the local buckling behaviour and the cross-sectional resistances. For the purposes of uniform load distribution, the ends of all the specimens were milled flat prior to the compressive testing to ensure good contact between the specimens and the loading end plates. A pair of specially developed end fixture clampers were designed and fabricated by wire-cutting process and a number of high strength bolts were used to connect the individual component and tighten the end of the specimen and the fixtures. The mechanism illustration of the specimen with the fixture at the end is demonstrated in Fig. 7(a). The compressive loading test was conducted in the Structural Engineering Research Laboratory of The Hong Kong Polytechnic University using MTS machine with capacity of 5000 kN. The test set-up comprised four 50mm range Linear Variable Displacement Transducers (LVDTs) to measure the end shortening of the stub columns, as shown in Fig. 7. An initial load of approximately 10.0 kN was applied to the specimens to eliminate possible gaps between the specimen and the bearing plate, if any. All the stub column tests were performed with displacement control at a constant loading speed of 0.2 mm/min, such loading speed resulted in similar loading strain rate to the initial loading strain rate of the tensile coupon tests. Moreover, strain gauges were affixed to the mid-height of each specimen to record the compressive strain in longitudinal direction. Three strain gauges were adhered to the surface of the flange at the mid-height and four strain gauges were amounted to the web with two strain gauges on each side. It should be noted that the records from the LVDTs necessarily contain the elastic deformations from the end plates and the deformation of the specimens. To obtain the true end shortening of the specimen, elastic deformation from the end plates should be eliminated. The deformation of each end plate was elastically proportional to the applied stress, and the true end shortening can be determined from the readings from the LVDTs and strain gauges by eliminating the end plates' deformation [30]. Hence, the readings from the strain gauges were utilized to modify the initial stage of the LVDT readings, removing the effect of the initial gaps and the elastic end plate deformation.

The load-axial end shortening curves of the tested HSS welded T-section stub columns are plotted in Fig. 8. Key experimental test results of the T-section stub column tests including the ultimate axial load N_u, the end shortening at ultimate load δ_u, yield load N_y and the ultimate to yield load ratio N_u/N_y are summarized in Table6. The ultimate to yield load ratio N_u/N_y was used to distinguish the specimen failed by cross-section yielding or local buckling. The specimen was considered to be failed by cross section yielding when the ratio of N_u/N_y is greater than the unity.

It is observed that for the stub column specimens failed by cross-section yielding, the load-axial end shortening curves exhibit comparably greater deformation capacity than the specimens which failed by local buckling. For those specimens failed by local buckling prior to the attainment of the squash load, the cross-section resistances feature with relative sharp drop after the ultimate resistance load. Photo of failed stub columns with representative failure modes are shown in Fig. 9. For the HSS welded T-section stub columns failed with either yielding failure or elastic local buckling, the failure modes display typical inward-outward local buckling in the constituent plate elements.

6. Numerical simulations

6.1 General

In parallel with the experimental tests, numerical simulations programme, including validation study and parametric study was conducted by means of finite element (FE) analysis software ABAQUS [31]. The primary aims of the numerical validation study are (i) to develop and to validate the FE model against the experimental results; (ii) subsequently to conduct the parametric studies using the validated FE models to generate further numerical data to supplement the test results.

6.2 Development of finite element models

The measured cross-section geometries given in Table. 3 were modeled for each stub column test. The mean measured Young's modulus and material properties obtained from the tensile coupon tests were used in FE models [1, 2]. In terms of material properties for HSS Q690 materials, the plastic material model with isotropic hardening, provided in ABAQUS [31] was employed. The input material behaviour was specified in terms of true stress and true plastic strain. The true stress and true plastic strain curves were converted from the mean engineering stress-strain curves from the coupon tests taken from the parent plate longitudinally and transversely in accordance with Eqs. (2) – (3).

$$\sigma_{\mathrm{true}} = \sigma_{\mathrm{eng}}(1+\varepsilon_{\mathrm{eng}}) \tag{2}$$

$$\sigma_{\mathrm{true}}^{\mathrm{pl}} = \ln(1+\varepsilon_{\mathrm{eng}}) - \left(\frac{\sigma_{\mathrm{true}}}{E_{\mathrm{s}}}\right) \tag{3}$$

where σ_{eng} and ε_{eng} are the engineering stress and engineering strain from tensile coupon tests, E_s is Young's modulus obtained from the tests, and σ_{true} and ε_{true}^{pl} are the true stress and plastic strain.

The element type chosen for numerical study is a four-node shell element with reduced integration, S4R, which has been extensively used in previous numerical modelling of welded sections [32, 33]. The element size was determined following a prior mesh sensitivity study with element size varying from $0.5t_w$ to $3t_w$. The results of the sensitivity study generally indicate that an element size equal to the thickness t_w can provide numerical accuracy and computational efficiency. The mesh was assigned uniformly along the longitudinal direction of the stub column specimen. With regard to the welded T-section boundary conditions, the two end sections of each stub column FE models were fully restrained against all degree of freedom except for the axial translation at the loaded end to mimic the fixed end boundary condition adopted in the stub column tests. Initial local geometric imperfections were incorporated into the FE models with the distributed profile taken as the lowest elastic buckling eigen mode under compression, as shown in Fig. 10. In particular, attention was also paid to the fillet welds to ensure that the properties of the fillet welds can be accurately represented. The nodes at the end of the web were shifted by a distance of half the flange thickness to avoid overlapping of the elements at the web-to-flange junction, these nodes were then tied to the mid thicknesses of the flange and the web by function of "General multi-point constraints (MPC)" which can ensure that the transitional and rotational degrees of freedom were equal for this pair of nodes. The geometries of the welding were accounted for using the additional shell elements with varying thicknesses, as shown in Fig. 11. The material properties of these elements were assumed to be the same as those of the web, which have been successfully applied in [39, 43]. Moreover, the membrane residual stress for HSS welded I-section proposed in [2] were transformed to T-sections and then incorporated into the FE models through the command of "INITIAL CONDITIONS". As the strips were also wire-cut from the I-sections and the predictive model was proposed in a symmetrical pattern [22] thus it may be also applied to T-section in this study due to the minimized thermal effect. The residual stress distribution mode for HSS T-section stub columns is depicted in Fig. 12. It should be noted that the net force of the T-section in predictive model is zero for T-section. For the purpose of assessing the sensitivity of the FE models to imperfections and seeking the most appropriate local imperfection magnitude, a total of four imperfection magnitudes including the measured local geometric imperfection value ω_0, and three investigated imperfection values expressed by the fraction of the web plate thickness ($t_w/10$, $t_w/50$, $t_w/100$) were adopted, to evaluate their influences on the numerical failure loads. The concentric compressive load was applied by specifying the axial displacement using a static RIKS step. The non-linear geometric command (*NLGEOM) was able to allow for large displacement analysis. A typical membrane residual stress distribution incorporated into the FE model for the stub column specimen T-SC-110 × 6 is presented in Fig. 13 with positive values indicating tensile membrane residual stress and negative values representing compressive membrane residual stress. To evaluate the impact of the membrane residual stress on the structural response, the magnitudes of membrane residual stress were explicitly incorporated into FE models of T-SC-110 × 6. The results obtained from FE model with inclusion of membrane residual stress were compared with the FE model without the inclusion of membrane residual stress. Fig. 14 presents the comparison of load-end shortening responses that the FE models with and without residual stress are almost identical with earlier yielding of the cross section observed for FE model with residual stress, indicating the influence of membrane residual stress on the structural response of welded T-section is negligible. For simplification, membrane residual stresses were not explicitly included in the FE model.

6.3 Validation of the FE models

Upon the development of FE models, the obtained failure modes, ultimate compressive loads, as well as the load-end shortening curves were compared with those obtained from the experimental tests to assess the accuracy of the models. Failure modes of the Q690 HSS welded T-section stub column observed from test results and FE models are presented in Fig. 15. Excellent agreement was obtained between the experimental observations and FE models. Figs. 16 depicts the comparisons between the experimental and numerical load-end shortening responses of stub columns of T-SC-80 × 6 where the full range of structural responses from numerical modelling are shown to correlate well with the counterparts from the experiments. Table 7 summarizes the FE-to-test failure load ratios for the Q690 HSS welded T-section stub column specimens. Mean values of $N_{u,FE}/N_{u,test}$ of the four considered initial local imperfection magnitudes are 1.02, 1.01, 1.02 and 1.03 respectively with corresponding

CoVs of 0.02, 0.03, 0.03 and 0.03. The comparisons and statistical analysis indicate that four cases of imperfection magnitudes generate precise and consistent predictions while the best agreement between the experimental and numerical was achieved when the imperfection amplitude equal to 1/10 of the plate thickness. It is however observed that the ultimate strength predictions from the FE simulations were relatively insensitive to the magnitude of the initial local geometric imperfections. This initial local imperfection value of $t_w/10$ was thereby used in further numerical simulations. Overall, it can be concluded that the developed FE models can yield accurate predictions which are capable of precisely simulating the failure modes, predicting the ultimate compressive loads as well as the load-end shortening curves of Q690 HSS welded T-section stub column specimens.

6.4 Parametric studies

Upon replicating the test results satisfactorily, the validated Q690 HSS welded T-section sub column FE models were adopted to conduct numerical parametric studies, aiming at expanding the numerical database to cover a wider range of cross-sectional slenderness to supplement the experimental results. In terms of the material properties in parametric studies, the average material properties of 6 mm thick and 10 mm thick plates are assigned to the corresponding plate elements respectively. The height of the fillet welds is used as the averaged value from tested specimens with value of 9 mm. The local imperfection magnitude of $t_w/10$ is used as discussed in section 6.3. With regard to the geometric dimensions of the modeled T-section specimens, the width of the flanges was fixed at 110 mm, while the widths of the web were taken as 60 mm, 110 mm and 150mm respectively, resulting in a larger spectrum of cross section aspect ratios. Furthermore, the thickness of the web of each modeled T-section varied from 3 mm to 15 mm, while the thicknesses of the flange were set to 6mm and 10 mm respectively, covering a broader range of cross-sectional dimensions. The length of each column was equal to three times of the outer cross section depth. A total of 88 FE models were developed in the parametric studies. The results of the parametric studies in conjunction with the test results were utilized to assess the design provisions specified in design codes for HSS welded sections. Detailed discussions and comparisons regarding the test results from parametric studies are given in the sub-sections of 7.2 and 7.3.

7. Evaluation of the existing design methods

7.1 General

In this section, the current codified design provisions and design methods were assessed against the 16 experimental data and 88 FE results for Q690 welded T-section stub columns. For the design codes, three structural steel design codes, namely the European code EN 1993-1-12 [17], American specification ANSI/AISC 360-16 [18] as well as Australian standard AS 4100 [19], were adopted for comparison and assessment in this study. The European code EN 1993-1-12 [17] covers the structural steel design provisions applicable for the HSS with nominal yield strength greater than 460 MPa and up to 700 MPa. Note however that the existing EN 1993-1-12 [17] is considered simply as an extension of the current EN 1993-1-1 [40] for conventional-strength steel with nominal yield strength less than or equal to 460 MPa. The design specifications of ANSI/AISC 360-16 [18] and AS 4100 [19] provide design provisions for HSS up to nominal yield strength of 690 MPa. For the stub columns under concentric compressive load, the concept of cross-section classification and the methodology of effective width method are employed to deal with the local buckling design of the stub columns at cross-section level. The accuracy of the slenderness limits for outstand-flange of the welded section in EN 1993-1-12 [17] and AS 4100 [19] are assessed, while the design provisions for T-section stipulated in ANSI/AISC 360-16 [18] is compared and assessed. In addition, the direct strength method (DSM) [20] originally developed for the stability design of the sections taking account of the element interaction is assessed, while the deformation-based design method, continuous strength method (CSM) [21], considering the interaction effect and strain-hardening of the metallic material is also evaluated. After assessing the classification limits for slender and non-slender cross sections, the cross-section compression resistance predictions regarding the Q690 welded T-sections are compared and assessed using effective width method as well as the DSM and CSM.

7.2 Cross-section classification limits

As mentioned in the previous section, the cross-section classification concept is adopted in all these three structural steel design codes. In accordance with the European EN 1993-1-12 [17], the cross-section classification is categorized into four classes. Class 1, 2 and 3 are the cross-sections capable of attaining the yield load Af_y, whereas Class 4 indicates those sections failed before attainment of the yield load due to the occurrence of elastic buckling. To address the Class 4 sections stability design, the area A is reduced to the effective area A_{eff}, resulting in an effective compression resistance resultant $A_{eff} \times f_y$. Likewise, the American specification ANSI/AISC 360-16 [18] and Australian standard AS 4100 [19] categorize the cross-sections in compression as non-slender and slender sections. Slender sections indicate the sections failed by local buckling failure prior to the achievement of the yield load Af_y, corresponding to the Class 4 sections codified in EN 1993-1-12 [17], whereas non-slender sections are the sections which can reach the yield strength before local buckling occurs, corresponding to the sections Class 1-3 specified in European code. According to the European code of EN 1993-1-12 [17], the Class of the cross section subject to compressive load is defined on the basis of its slenderest constituent plate element with each plate element classified by comparing the width-to-thickness ratio c/t with codified slenderness limits, where c is the clear width of the plate element. The slenderness limits codified in those design codes applicable to T-sections are summarized in Table. 8. To consider the effect of the high strength materials, the material parameters of $\varepsilon_{EC3} = (235/f_y)^{0.5}$, $\varepsilon_{AISC} = (E/f_y)^{0.5}$, and $\varepsilon_{AS4100} = (250/f_y)^{0.5}$ are used to account for the differences of the material strengths. The compression resistance from the experimental results in this study and the numerical data generated from the FE models of the HSS welded T-sections are normalized to the corresponding cross-section yield load Af_y and subsequently plotted against the ratios of $c/(t\varepsilon_{EC3})$, $c/(t\varepsilon_{AISC})$ and $c/(t\varepsilon_{AS4100})$ of the governing outstand flange of the T-sections in Fig. 17. Note that the Class 3 limit in European code, yield slenderness limit in American AISC code and the limiting width-to-thickness ratio in Australian code AS 4100 are also plotted for comparison purposes in Fig. 17.

To eliminate the limitation in finding the effective width with iterated process in effective width method, the DSM was developed by Schafer and Pekoz [20] which is applicable to arbitrary cross-sections for critical elastic buckling stress predictions. DSM relies on the estimation of elastic local, global and distortional buckling stress by employing the numerical software such as finite strip method software CUFSM or finite element method, ABAQUS [31]. The DSM for compressive member design has been included and detailed in Chapter E of the AISI-S100 [41]. A non-dimensional cross-section slenderness parameter $\lambda_p = (f_y/f_{cr})^{0.5}$ is used in DSM by which the resistance of the structural member can be derived based on the developed strength curves, where f_y is the yield strength of the steel material, f_{cr} is the elastic buckling stress.

$$N_{DSM}\begin{cases} f_y A & \text{for } \lambda_p \le 0.776 \\ (1-\dfrac{0.15}{\lambda_p^{\ 0.8}})\dfrac{1}{\lambda_p^{\ 0.8}} f_y A & \text{for } 0.776 < \lambda_p \end{cases} \tag{4}$$

To consider the strain hardening of the metallic material, CSM was developed that cross-section classification and calculation of the effective width are not needed in determining the compressive strength [21, 42]. The relationship between the cross-sectional slenderness parameter $\lambda_p = (f_y/f_{cr})^{0.5}$ and the deformation capacity ($\varepsilon_{CSM}/\varepsilon_y$) is described by the base curve. To address the local buckling, base curve has been developed based on carbon and stainless-steel column and beam tests [34, 35]. The deformation capacity ε_{CSM} is normalized to the yield strain ε_y

= (f_y/E). For HSS structural elements, base curve developed for HSS under compressive load in [36] is used in this study, shown as follows,

$$\begin{cases} \dfrac{\varepsilon_{\mathrm{csm}}}{\varepsilon_{\mathrm{y}}} = \dfrac{0.294}{\lambda_{\mathrm{p}}^{3.174}} \leq \min(15, \dfrac{C_1 \varepsilon_{\mathrm{u}}}{\varepsilon_{\mathrm{y}}}) & \text{for } \lambda_{\mathrm{p}} \leq 0.68 \\ \dfrac{\varepsilon_{\mathrm{csm}}}{\varepsilon_{\mathrm{y}}} = (1 - \dfrac{0.219}{\lambda_{\mathrm{p}}^{1.014}}) \dfrac{1}{\lambda_{\mathrm{p}}^{1.014}} & \text{for } 0.68 < \lambda_{\mathrm{p}} \end{cases} \quad (5)$$

The comparisons generally demonstrate that the current codified slenderness limits in EN 1993-1-12 [17], ANSI/AISC 360-16 [18] as well as AS 4100 [19] for slender/non-slender outstand flat elements are safe and accurate for classification of the HSS welded T-section under compression. Three scattered data points in Fig. 17 are due to the interaction effect between the constituent plate elements. The cross-sectional slenderness limit adopted in DSM ($\lambda_p = 0.776$) is relatively accurate for HSS T-section, as shown in Fig. 18.

7.3 Cross-section compression resistances

In this section, the accuracy of the compression predictions determined from the design codes and the design methods are assessed and evaluated. Note that all these three structural steel design codes stipulate the compression resistance of yield load Af_y for non-slender sections or Class 1-3 sections while effective width method was adopted to deal with the sections with occurrence of buckling prior to attainment of the yield load for slender sections or Class 4 counterparts. Note that the EN 1993-1-12 [40], ANSI/AISC 360-16 [19] and AS 4100 [20] use different expressions to determine the effective width of the slender plate elements subject to local buckling, as given in Eqs. (6) – (8),

$$c_{\mathrm{eff,EC3}} = c(\frac{1}{\bar{\lambda}_{\mathrm{p}}} - \frac{0.188}{\bar{\lambda}_{\mathrm{p}}^{2}}) \leq c \quad (6)$$

$$c_{\mathrm{eff,AISC}} = c(\frac{1.49\lambda_{\mathrm{p,AISC}}}{c/t} - \frac{0.49\lambda_{\mathrm{p,AISC}}^{2}}{(c/t)^2}) \leq c \quad (7)$$

$$c_{\mathrm{eff,AS4100}} = c(\frac{14}{c/(t\varepsilon_{\mathrm{AS4100}})}) \leq c \quad (8)$$

where $\lambda_{p,AISC}$ is the AISC limiting width-to-thickness ratio for outstand plate element, and plate element slenderness codified in EN 1993-1-12 [17] can be derived and is given in Eq. (9)

$$\bar{\lambda}_{\mathrm{p}} = \frac{c/t}{28.4\varepsilon_{\mathrm{EC3}}\sqrt{k_{\sigma}}} \quad (9)$$

where k_σ is the buckling factor taken as 0.43 for outstand plate element in compression.
The resistance prediction from DSM for structural members under compressive load has been introduced, whereas for the prediction based on CSM, the CSM design stress f_{csm}, strain hardening slope E_{sh} and the predicted strain ε_u corresponding to the ultimate stress are needed. To obtain these parameters, the expressions expressed by Eqs. (10) – (14) developed for HSS in [37] for nominal yield strength of 690 MPa and $f_y/f_u > 0.9$ is used and assessed in this study.

$$f_{\mathrm{csm}} = f_{\mathrm{y}} + E_{\mathrm{sh}}\varepsilon_{\mathrm{y}}(\frac{\varepsilon_{\mathrm{csm}}}{\varepsilon_{\mathrm{y}}} - 1) \quad (10)$$

$$E_{\mathrm{sh}} = \frac{f_{\mathrm{u}} - f_{\mathrm{y}}}{C_2\varepsilon_{\mathrm{u}} - \varepsilon_{\mathrm{y}}} \quad (11)$$

$$\varepsilon_u = 1 - \frac{f_y}{f_u} \quad (12)$$

$$C_2 = \frac{\varepsilon_{sh} + 0.55(\varepsilon_u - \varepsilon_{sh})}{\varepsilon_u} \quad (13)$$

$$\varepsilon_{sh} = -0.2\frac{f_y}{f_u} + 0.2 \quad (14)$$

The constant C_1 and C_2 are the material related coefficients. Upon determination of the CSM design stress f_{csm}, the stub column capacity is derived based on the gross cross-section area, as given in Eq. (15)

$$N_{csm} = \begin{cases} f_{csm}A & \text{for } \lambda_p \leq 0.68 \\ \frac{\varepsilon_{csm}}{\varepsilon_y} f_y A & \text{for } \lambda_p > 0.68 \end{cases} \quad (15)$$

The experimental data together with the data generated from the FE models of HSS welded T-section stub column specimens are normalized by the design compression capacities predicted from the standards and the resistance predictions generated from DSM as well as CSM. The normalized strengths are then plotted against the corresponding normalized plate slenderness, as shown in Figs. 19 – 23. The cross-section strength predictions determined from the design codes and design methods are normalized to the experimental data. In terms of the cross-section strength comparisons between the design codes and the design methods, relatively close predictions are provided from AISC 360-16 and DSM, but relatively higher CoV of DSM is observed. The mean values of $N_u/N_{,pred}$ obtained from EN 1993-1-12, AISC 360-16, AS4100, DSM and CSM are 1.08, 1.06, 1.11, 1.06 and 1.11 with corresponding CoVs of 0.02, 0.05, 0.01, 0.06 and 0.08. Table. 9 summarizes the results of the statistical analysis of the cross-section resistance predictions, including the mean (test and FE)- to-predicted compression resistance ratios $N_u/N_{u,pred}$, the corresponding coefficient of variations (CoVs), as well as the reliability analysis indexes. The reliability analysis was conducted in accordance with EN 1990 [38]. The material over-strength $f_{y,mean}/f_{y,nom}$ =1.15 derived in [37] is used with CoV of the geometric properties taken as 0.05. V_δ is the CoV of the test and FE results relative to the design model. V_r is the combined CoV incorporating both model and basic variable uncertainties. γ_{M0} is the partial safety factor for cross section resistance, whereas the γ_{M0}^* is the corrected partial factor. The mean values of $N_u/N_{u,pred}$ obtained from EN 1993-1-12, AISC 360-16, AS4100, DSM and CSM are 1.06, 1.05, 1.09, 1.08 and 1.12 with corresponding CoVs of 0.05, 0.06, 0.15, 0.14 and 0.13. The results demonstrate that both design codes of EN 1993-1-12 and AISC 360-16 yield relatively accurate and consistent predictions of cross section compressive resistance than AS 4100, DSM, and CSM for Q690 welded T-section stub columns.

8. Conclusions

Experimental and numerical investigations into the stub column behaviour of HSS welded T-section has been presented in this paper. A total of 16 Q690 HSS welded T-section stub column specimens were conducted under concentric compressive load. Tensile coupon specimens were extracted from the parent plates to determine the material properties of the HSS. Initial local geometric imperfections for each cross section were measured. In conjunction with the experimental study, finite element (FE) models were developed using commercially available software ABAQUS [27] to replicate the test results in this study. Residual stresses were found to have negligible effect on the ultimate capacity. The validated FE model was adopted to conduct parametric study to complement the test database covering a wider spectrum of cross-sectional slenderness. The obtained test and FE results were used to assess the accuracy of the slenderness limits for classifications of Q690 high-strength steel outstand plate elements in compression and the local buckling design rules given in EN 1993-1-12, ANSI/AISC 360-16, AS 4100 as well as DSM. For resistance predictions, CSM was also assessed with reliability analysis conducted for all design standards and design methods in accordance with EN 1990. It should be noted that the following conclusions can be drawn:

(a) The results of the assessment generally indicate that the codified slenderness limits in the three design standards and the limit value specified in DSM are safe and accurate when applied to Q690 HSS welded T-section in compression. The classification limits in the current structural design codes can be directly used for HSS welded T-section.

(b) It is shown that strength predictions from EN 1993-1-12 and ANSI/AISC 360-16 generally provide relatively satisfactory results in comparison with the AS 4100 counterpart. Though ANSI/AISC 360-16 yield more accurate predictions, EN 1993-1-12 provide more consistent cross-section strength predictions with less scatted data.

(c) The most accurate predictions for cross-section resistance are provided by ANSI/AISC 360-16 with relatively lower coefficient of variation value than AS 4100 and design approaches of DSM and CSM.

(d) Cross-section resistance predictions generated from DSM and CSM generally tend to underestimate the capacities for Q690 HSS welded T-section stub columns. Over-conservative results impede the application of design approach to T-section stub columns. Modified coefficients in design equations of DSM can resolve the over-conservatism which is currently under way.

(e) The underestimations from CSM may be primarily due to that CSM rely on a base curve of the structural member with specified cross section and it is originally developed for cold-formed stainless steel tubular sections with material properties exhibiting significant strain hardening. In this study, the material properties show limited strain hardening and the base curve employed was developed on the basis of HSS tubular sections, implying suitable base curve equation corresponding to T-section should be further investigated and developed.

Though reliable cross-section strength predictions are provided by three structural steel codes, relatively conservative results are observed. To improve the efficiency of structural steel design, design methods and effective width equation stipulated in those design codes, further investigation should be carried out with suitable improvements and modifications, which is currently under way.

Acknowledgement

The research work presented in this paper was supported by the Chinese National Engineering Research Centre for Steel Construction (Hong Kong Branch) at The Hong Kong Polytechnic University. The authors would also like to thank the technical staff, Mr. H.Y. Leung, Mr. K.H. Wong of the Structural Engineering Research Laboratory for their support as well as the support from the Industrial Center at The Hong Kong Polytechnic University.

References

[1] Zhang L, Wang F, Liang Y, Zhao O. Press-braked S690 high strength steel equal-leg angle and plain channel section stub columns: Testing, numerical simulation and design. Eng Struc. 2019;201:109764.
[2] Sun Y, Liang Y, Zhao O. Testing, numerical modelling and design of S690 high strength steel welded I-section

stub columns. J Constr Steel Res. 2019;159:521-33.
[3] Nishino F, Ueda Y, Tall L. Experimental investigation of the buckling of plates with residual stresses. Test methods for compression members: ASTM International; 1967.
[4] Nishino F, Tall L. Experimental investigation of the strength of T-1 steel columns: Fritz Engineering Laboratory, Department of Civil Engineering, Lehigh University; 1970.
[5] Rasmussen KJ, Hancock GJ. Plate slenderness limits for high strength steel sections. J Constr Steel Res. 1992;23:73-96.
[6] Shi G, Wang J, Bai Y, Shi Y. Experimental study on seismic behavior of 460MPa high strength steel box-section columns. Adv Struct Eng. 2014;17:1045-59.
[7] Schillo N, Feldmann M. Interaction of local and global buckling of box sections made of high strength steel. Thin-Walled Struct. 2018;128:126-40.
[8] Su A, Sun Y, Liang Y, Zhao O. Membrane residual stresses and local buckling of S960 ultra-high strength steel welded I-section stub columns. Thin-Walled Struct. 2021;161:107497.
[9] Sun Y, He A, Liang Y, Zhao O. In-plane bending behaviour and capacities of S690 high strength steel welded I-section beams. J Constr Steel Res. 2019;162:105741.
[10] Bartsch H, Eyben F, Pauli G, Schaffrath S, Feldmann M. Experimental and Numerical Investigations on the Rotation Capacity of High-Strength Steel Beams. J Struct Eng. 2021;147:04021067.
[11] Ma JL, Chan TM, Young B. Experimental Investigation on Stub-Column Behavior of Cold-Formed High-Strength Steel Tubular Sections. J Struct Eng. 2016;142.
[12] Wang J, Afshan S, Schillo N, Theofanous M, Feldmann M, Gardner L. Material properties and compressive local buckling response of high strength steel square and rectangular hollow sections. Eng Struc. 2017;130:297-315.
[13] Gkantou M, Theofanous M, Wang J, Baniotopoulos C, Gardner L. Behaviour and design of high-strength steel cross-sections under combined loading. Proc Inst Civil Eng-Struct Build. 2017;170:841-54.
[14] Meng X, Gardner L. Testing of hot-finished high strength steel SHS and RHS under combined compression and bending. Thin-Walled Struct. 2020;148:106262.
[15] Wang F, Zhao O, Young B. Testing and numerical modelling of S960 ultra-high strength steel angle and channel section stub columns. Eng Struc. 2020;204:109902.
[16] Cao X, Gu L, Kong Z, Zhao G, Wang M, Kim S-E et al. Local buckling of 800 MPa high strength steel welded T-section columns under axial compression. Eng Struc. 2019;194:196-206.
[17] EN 1993-1-12, Eurocode 3: Design of Steel Structures – Part 1–12: Additional Rules for the Extension of EN 1993 up to Steel Grades S700. Brussels: European Committee for Standardization (CEN); 2007.
[18] ANSI/AISC 360-16, Specification for Structural Steel Buildings. Chicago: American Institute of Steel Construction (AISC); 2016.
[19] AS 4100-1998(R2016), Steel structures (Reconfirmed 2016 Incorporating Amendment No.1), AS 4100. Sydney, Australia: Australian Standard; 2016.
[20] Schafer B, Peköz T. Computational modeling of cold-formed steel: characterizing geometric imperfections and residual stresses. J Constr Steel Res. 1998;47:193-210.
[21] Gardner L, Ashraf M. Structural design for non-linear metallic materials. Eng Struc. 2006;28:926-34.
[22] Ban H, Shi G, Bai Y, Shi Y, Wang Y. Residual stress of 460 MPa high strength steel welded I section: experimental investigation and modeling. Int J Steel Struct. 2013;13:691-705.
[23] GB/T 1591-2018. High strength low alloy structural steels, General Administration of Quality Supervision, and Standardization Administration of the People's Republic of China, Beijing, China, 2018
[24] Liu X, Chung K-F, Ho H-C, Xiao M, Hou Z-X, Nethercot DA. Mechanical behavior of high strength S690-QT steel welded sections with various heat input energy. Eng Struc. 2018;175:245-56.
[25] Amraei M, Ahola A, Afkhami S, Björk T, Heidarpour A, Zhao X-L. Effects of heat input on the mechanical properties of butt-welded high and ultra-high strength steels. Eng Struc. 2019;198:109460.

[26] Liu J-Z, Fang H, Chen S, Chan T-M. Material properties and residual stresses of high strength steel hexagonal hollow sections. J Constr Steel Res. 2022; 190, 107061.
[27] Liu J-Z. Fang H, Chan T-M. Material properties and residual stresses of high strength steel irregular octagonal hollow sections, J. Constr. Steel. Res. 2022; 107170. (In press)
[28] EN ISO 6892-1, Metallic Materials – Tensile Testing Part 1: Method of Test at Ambient Temperature. EN ISO 6892-1. Brussels, Belgium: CEN; 2019.
[29] Chen J, Zhu J-Y, Chan T-M. Experimental and numerical investigation on stub column behaviour of cold-formed octagonal hollow sections. Eng Struc. 2020;214:110669.
[30] Gardner L, Nethercot DA. Experiments on stainless steel hollow sections—Part 1: Material and cross-sectional behaviour. J Constr Steel Res. 2004;60:1291-318.
[31] ABAQUS/Standard. Version 6.14-1. U.S.A.: K. a. S. Hibbit.
[32] Fang H, Chan T-M, Young B. Behavior of octagonal high-strength steel tubular stub columns. J Struct Eng. 2019;145:04019150.
[33] Ma T-Y, Hu Y-F, Liu X, Li G-Q, Chung K-F. Experimental investigation into high strength Q690 steel welded H-sections under combined compression and bending. J Constr Steel Res. 2017;138:449-62.
[34] Buchanan C, Gardner L, Liew A. The continuous strength method for the design of circular hollow sections. J Constr Steel Res. 2016;118:207-16.
[35] Zhao O, Gardner L, Young B. Behaviour and design of stainless steel SHS and RHS beam-columns. Thin-Walled Struct. 2016;106:330-45.
[36] Lan X, Chen J, Chan T-M, Young B. The continuous strength method for the design of high strength steel tubular sections in compression. Eng Struc. 2018;162:177-87.
[37] Chen S, Fang H, Liu J-Z, Chan T-M. Design for local buckling behaviour of welded high strength steel I-sections under bending. Thin-Walled Struct. 2022;172:108792.
[38] EN 1990. Eurocode - Basis of structural design. Brussels, Belgium: European Committee for Standardization (CEN); 2002.
[39] Tse K, Wang J, Yun X. Structural behaviour and continuous strength method design of high strength steel non-slender welded I-section beam-columns. Thin-Walled Struct. 2021;169:108273.
[40] EN 1993-1-1, Eurocode 3: Design of Steel STRUCTURES – Part 1.1: General Rules and Rules for Buildings. Brussels: European Committee for Standardization (CEN); 2005.
[41] AISI S100-16, North American Specification for the Design of Cold-Formed Steel Structural Members. Washington, DC, USA: AISI (American Iron and Steel Institute); 2016.
[42] Yun X, Gardner L, Boissonnade N. Ultimate capacity of I-sections under combined loading – Part 2: Parametric studies and CSM design. J Constr Steel Res. 2018;148:265-74.
[43] Yun X, Gardner L, Boissonnade N. The continuous strength method for the design of hot-rolled steel crosssections. Eng Struc. 2018;157:179-91.

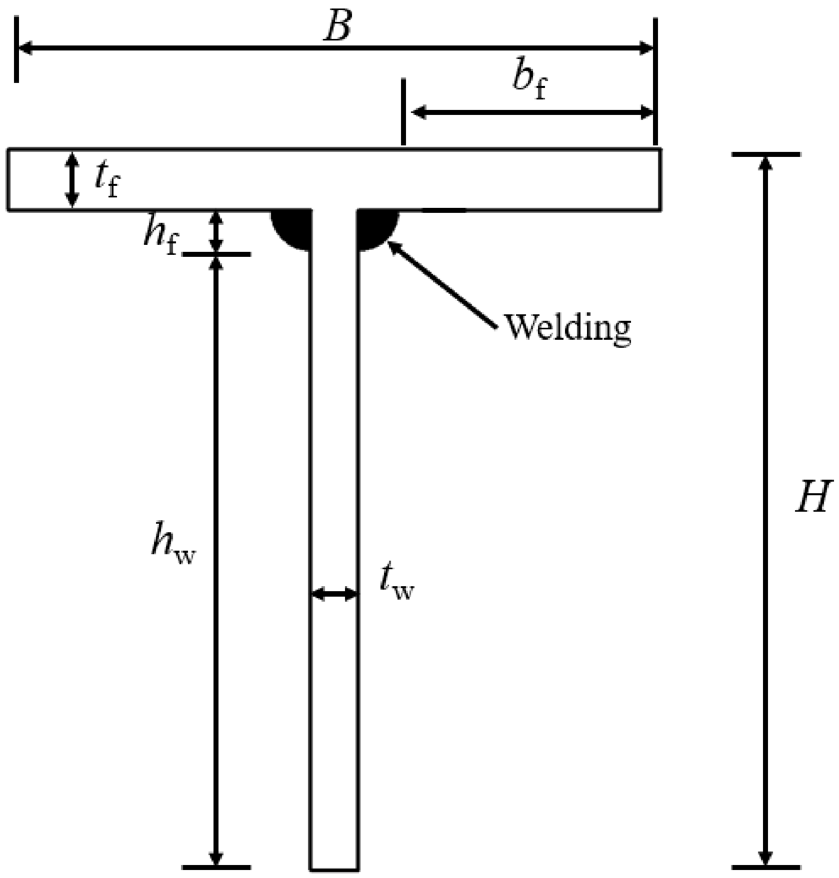

Fig. 1. Notations of the Q690 HSS welded T-section

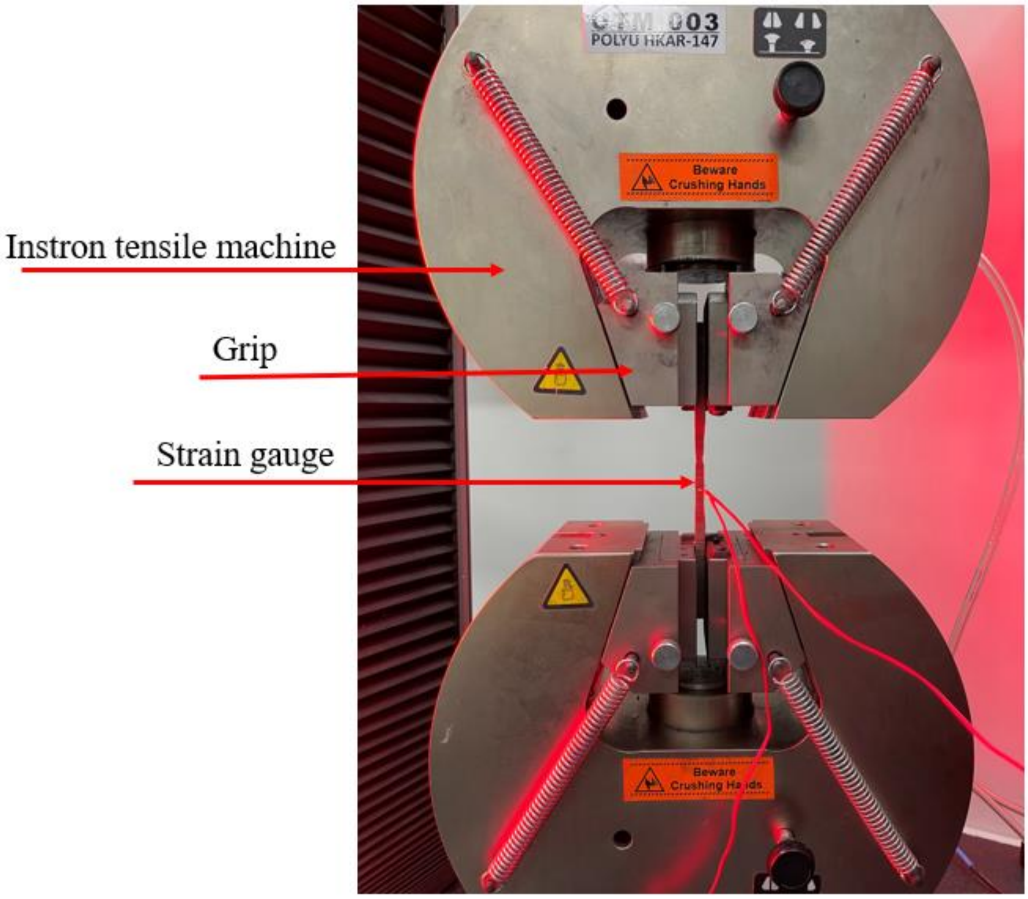

Fig. 2 Test arrangement of the tensile coupon specimen

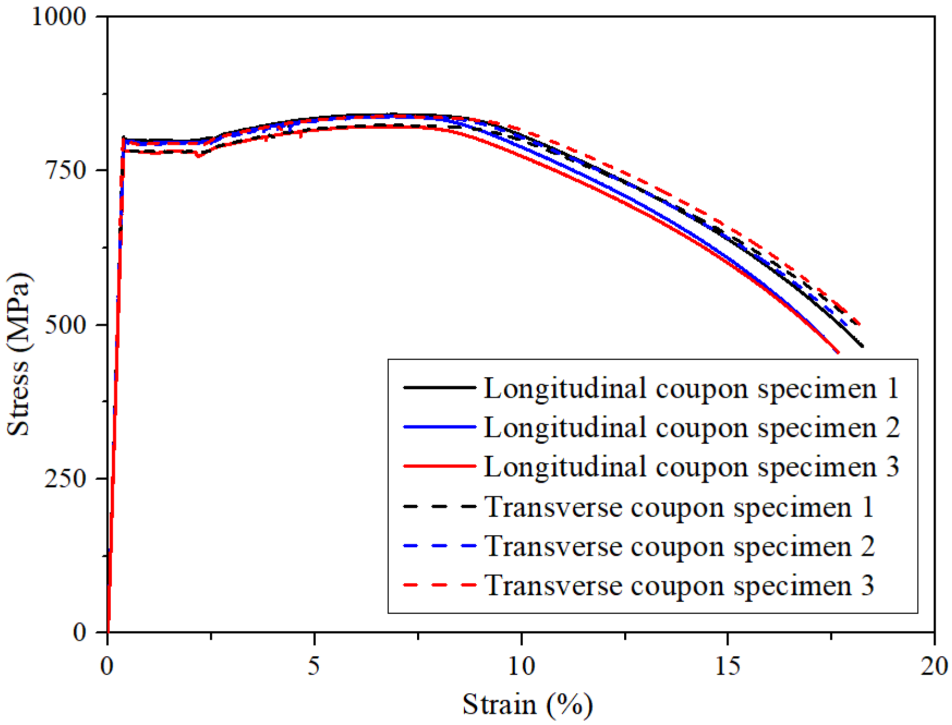

Fig. 3 Measured material stress-strain curves of Q690 high strength steel longitudinal and transverse tensile coupons extracted from 6 mm thick parent plate

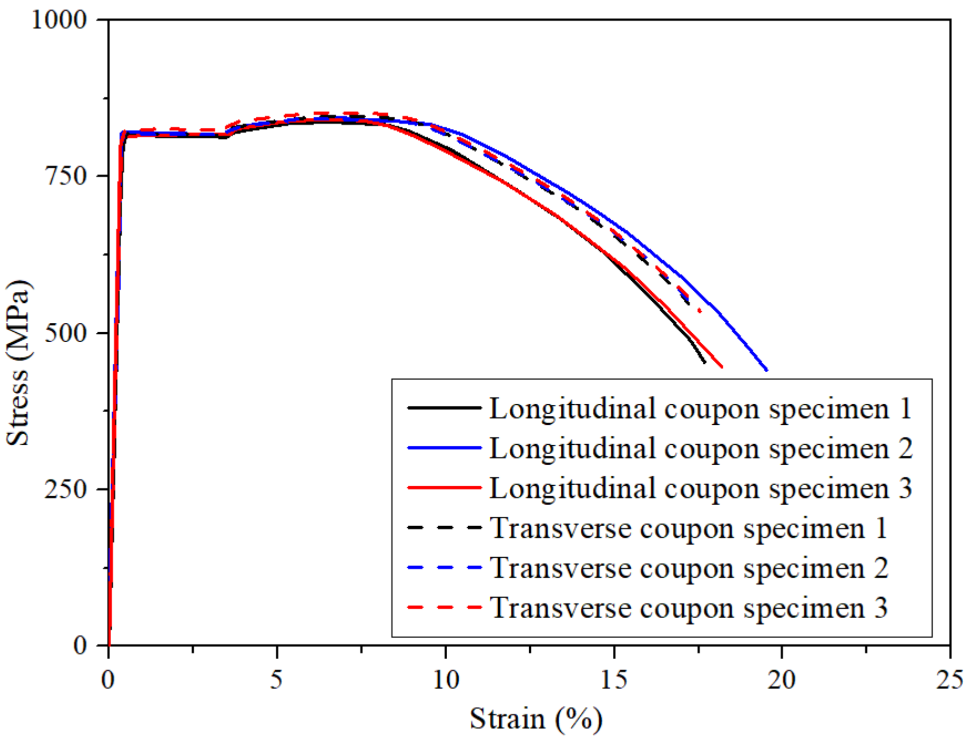

Fig. 4 Measured stress-strain curves of Q690 high strength steel longitudinal and transverse tensile coupons of 10 mm parent plate

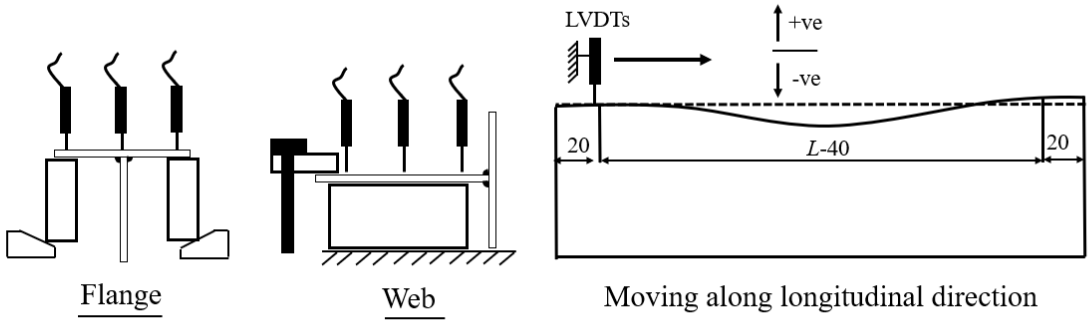

(a) Schematic view

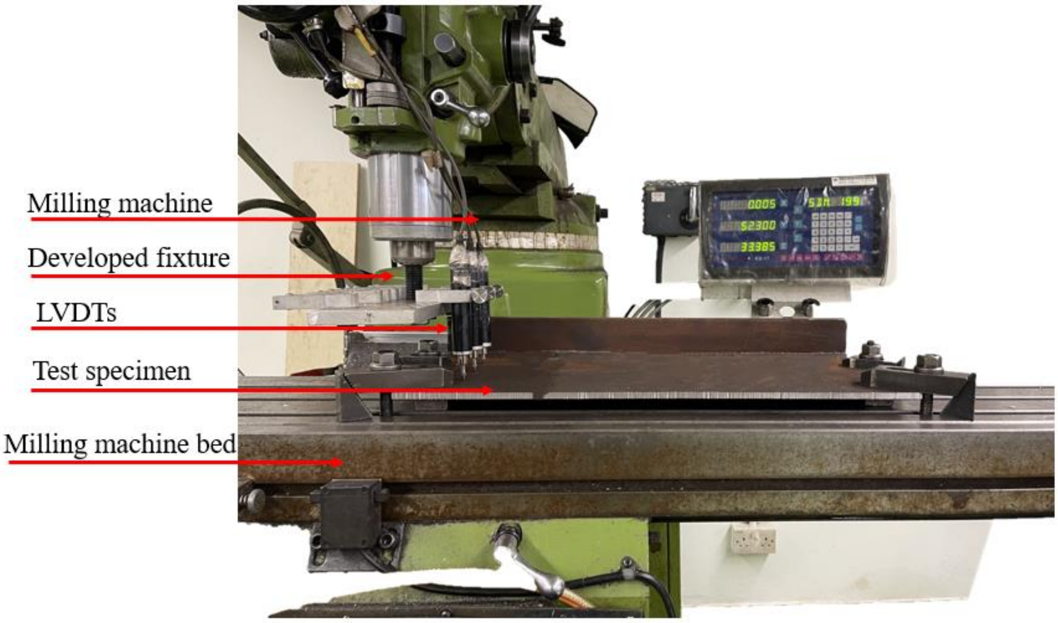

(b) Experimental arrangement

Fig. 5 Setup of local geometric imperfection measurements for HSS welded T-section

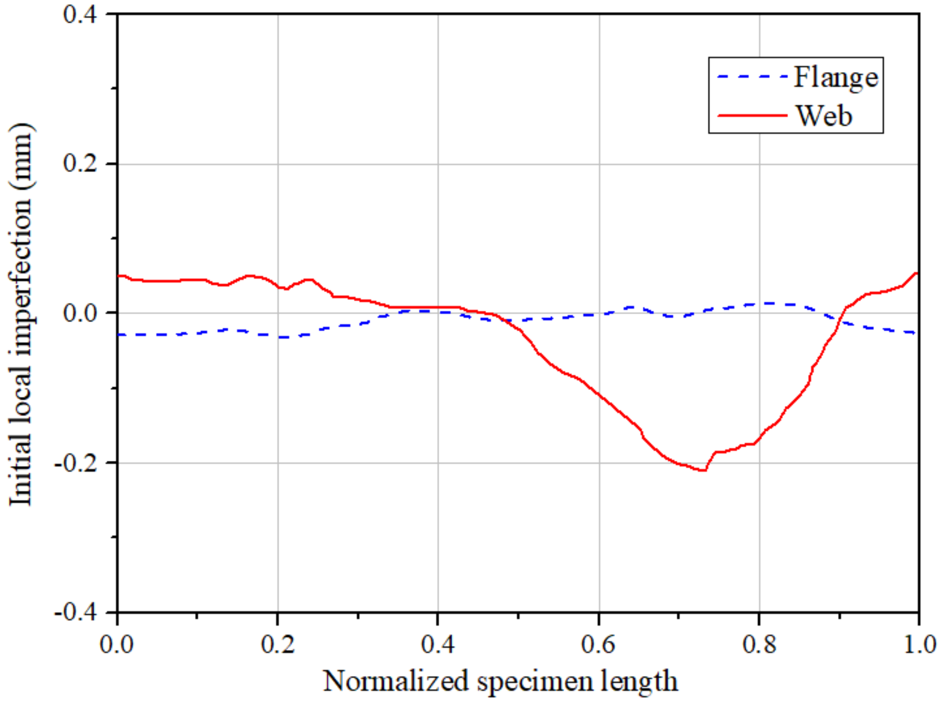

Fig. 6 The distribution of the initial local geometric imperfections along the length of the stub column specimen T-SC-100 × 6#

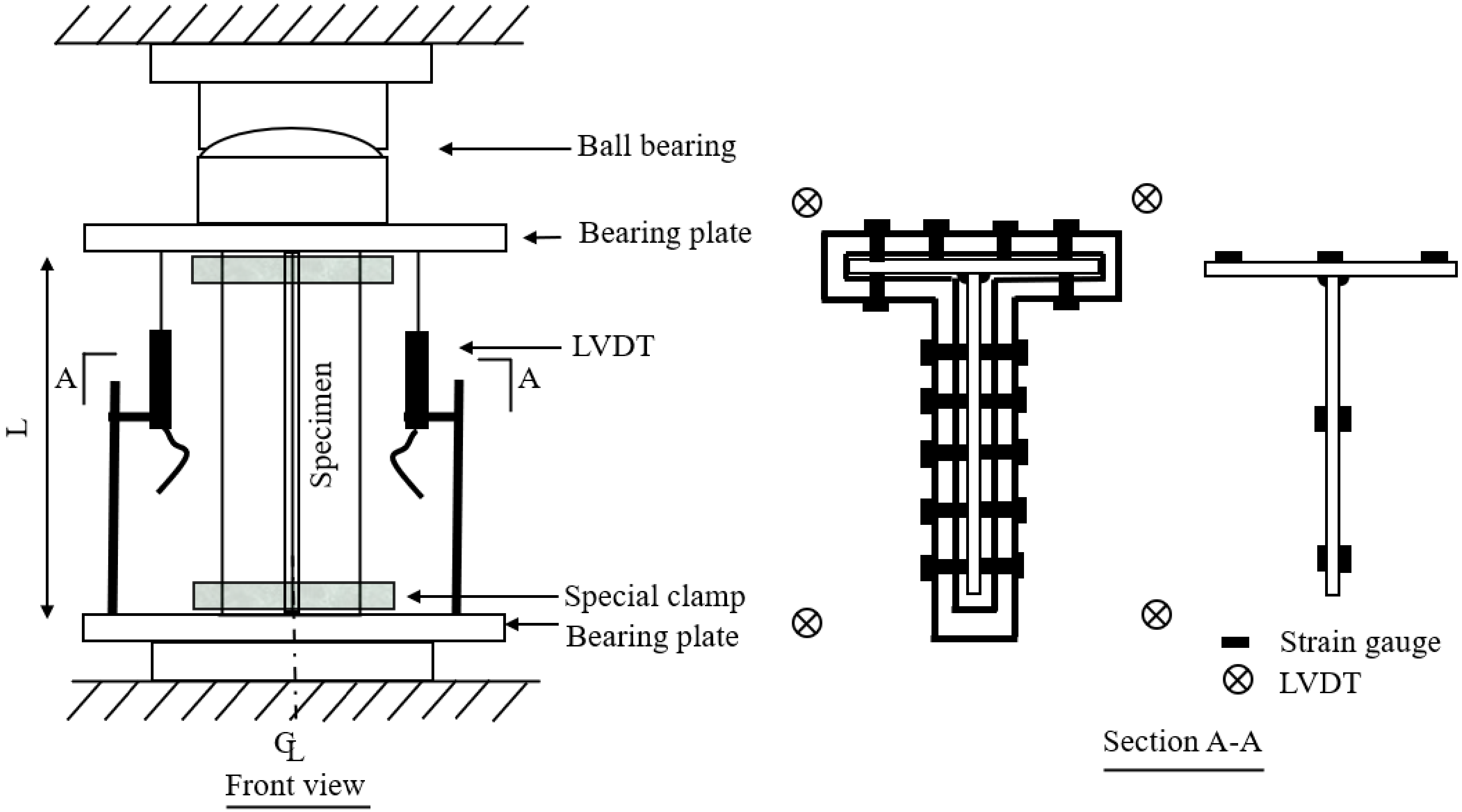

(a) Schematic arrangement

(b) Experimental arrangement

Fig. 7 Test set-up for HSS T-section stub columns

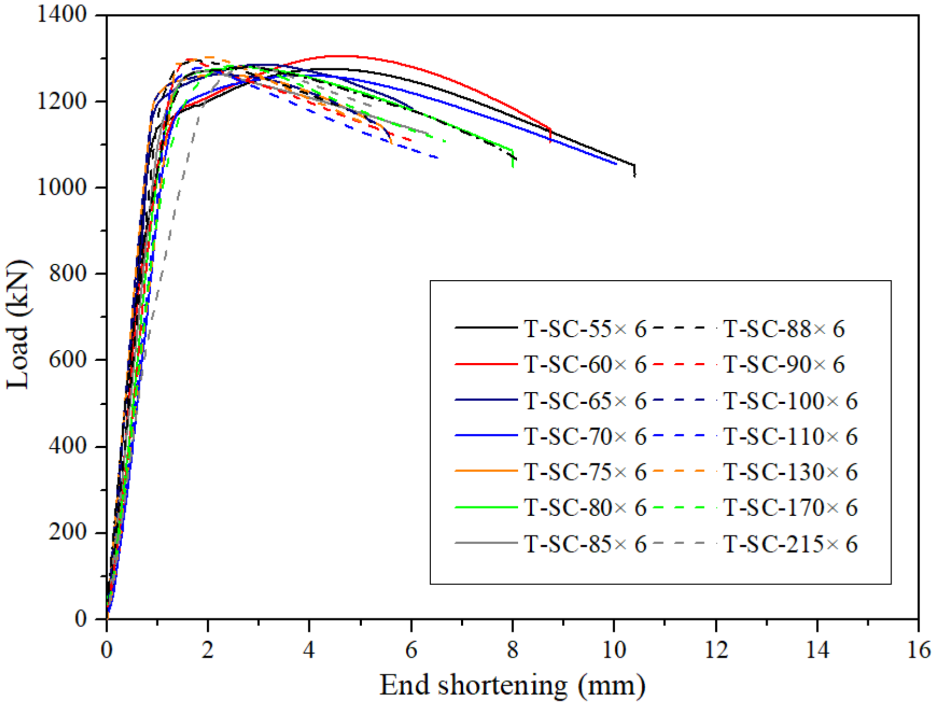

Fig. 8 Load-end shortening curves of Q690 HSS welded T-section stub columns

Fig. 9 Experimental failure modes of the representative Q690 HSS welded T-section stub columns

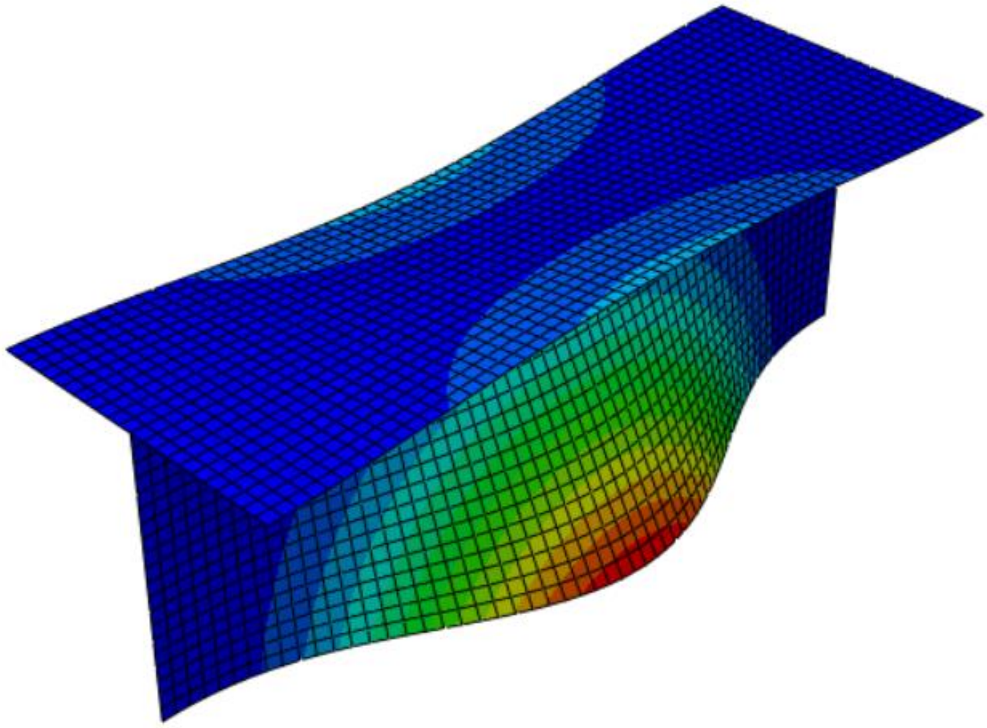

Fig. 10 The lowest eigenmodes of the stub column specimen

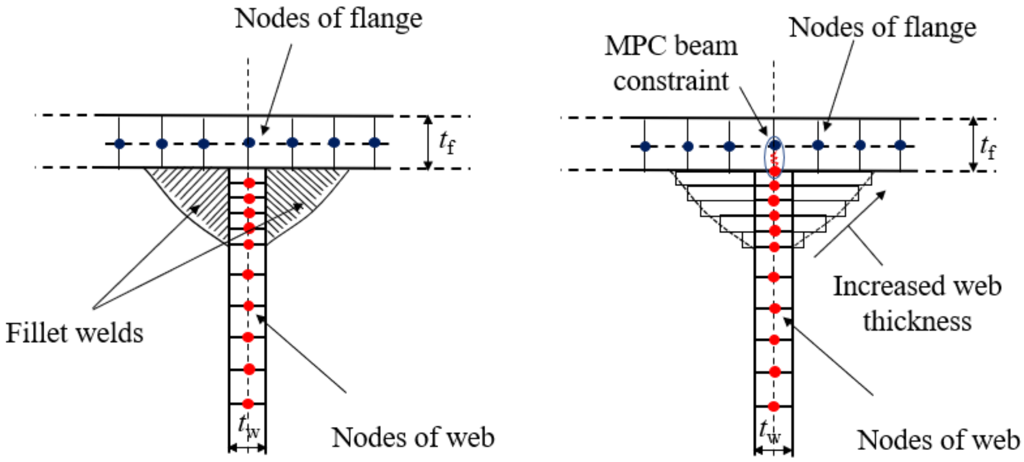

Fig. 11 FE modelling of fillet welds in welded T-section stub columns

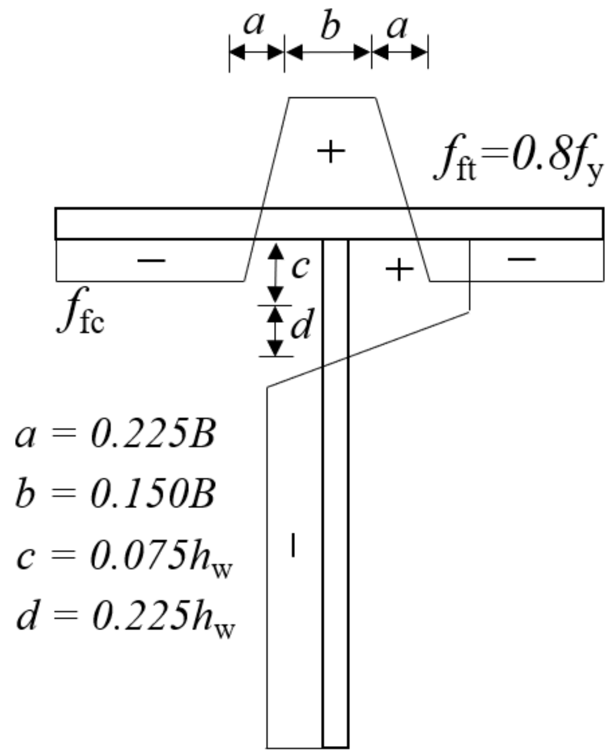

Fig. 12 Predictive model for membrane residual stress distribution

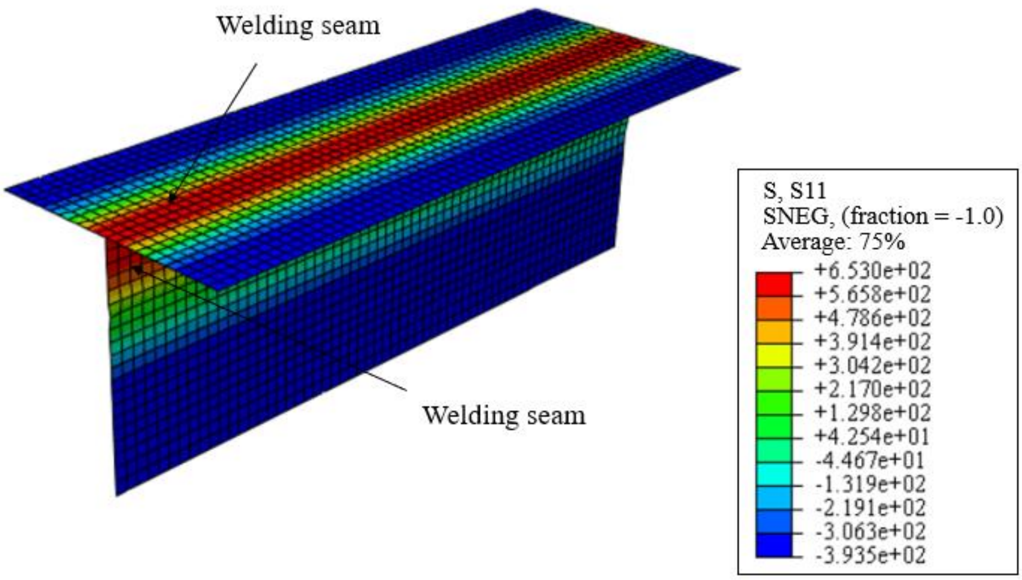

Fig. 13 Typical membrane residual stress distribution and amplitudes (in MPa) in modelled Q690 HSS welded T-section stub columns T-SC-110 × 6

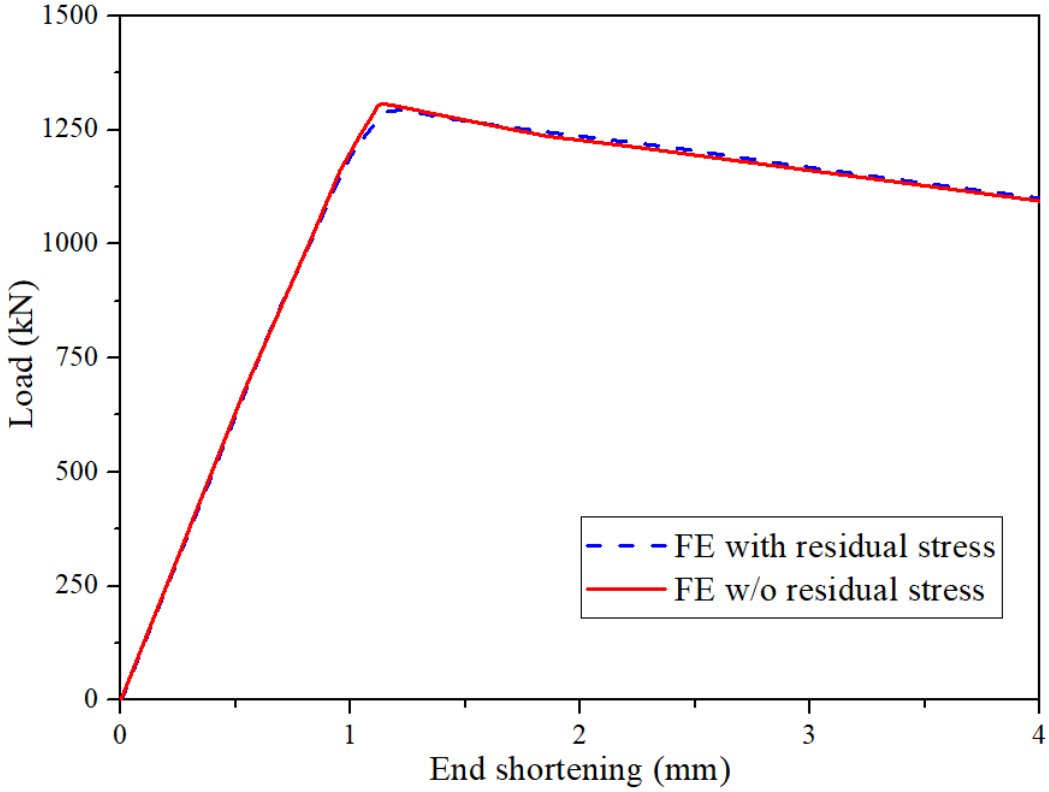

Fig. 14 Effect of membrane residual stress on Q690 HSS welded T-section stub columns T-SC-110 × 6

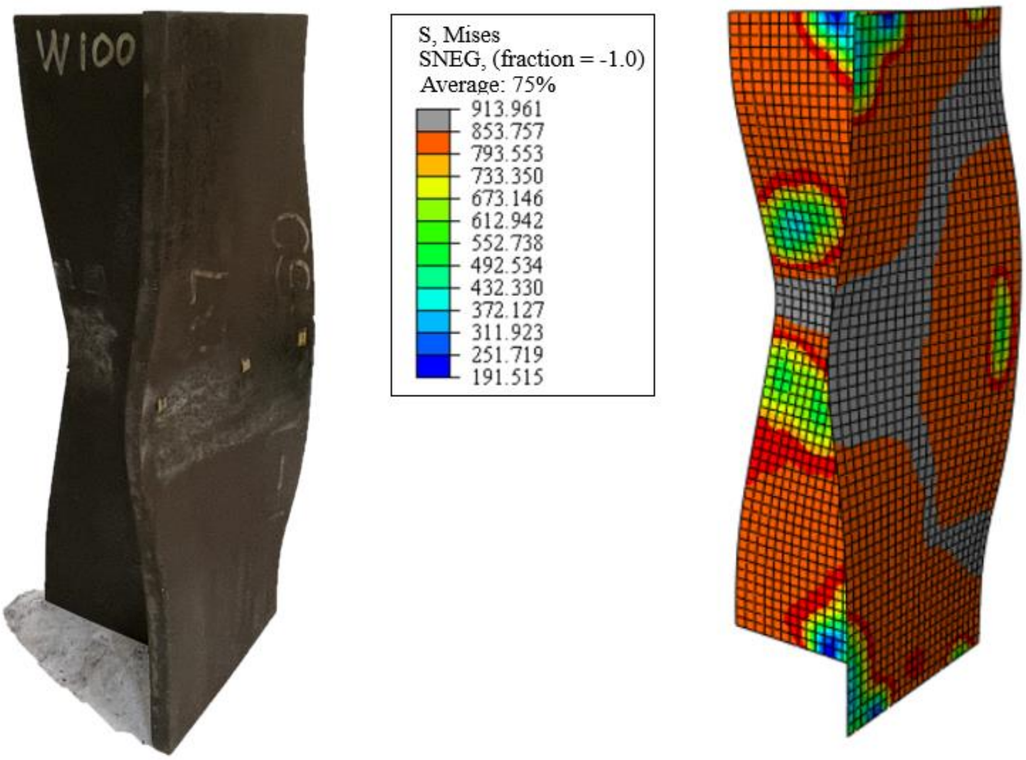

(a) Q690 HSS welded T-section stub column specimen T-SC-100 × 6 (legend unit in MPa)

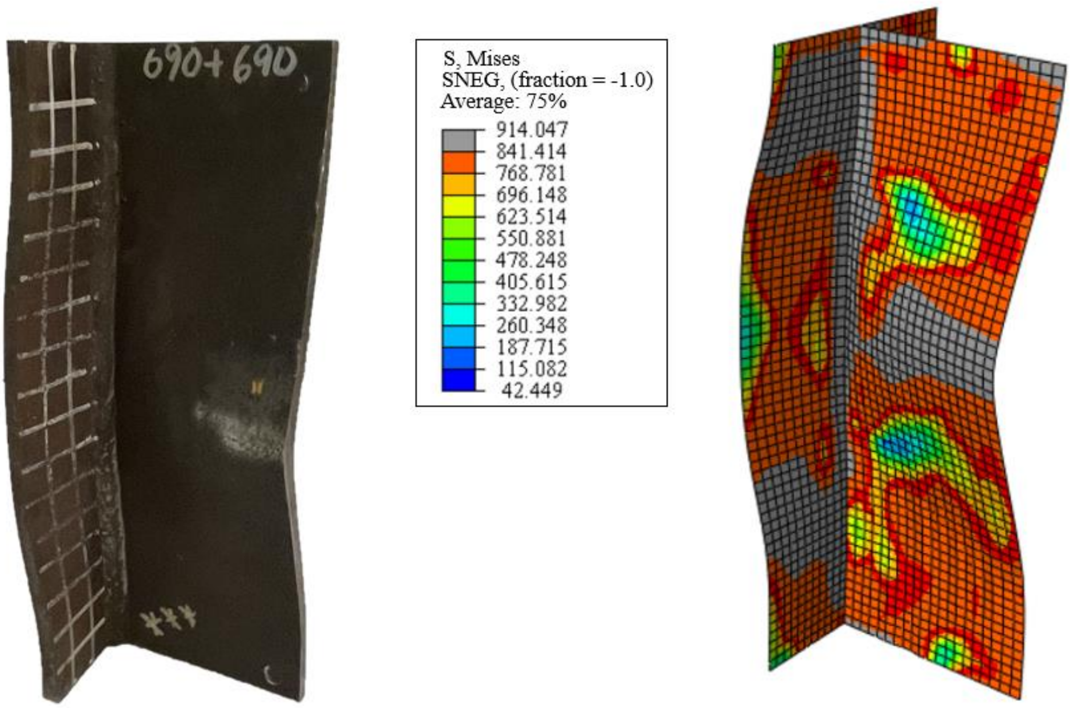

(b) Q690 HSS welded T-section stub column specimen T-SC-130 × 6 (legend unit in MPa)

Fig. 15 Test and FE failure modes for typical stub column specimens

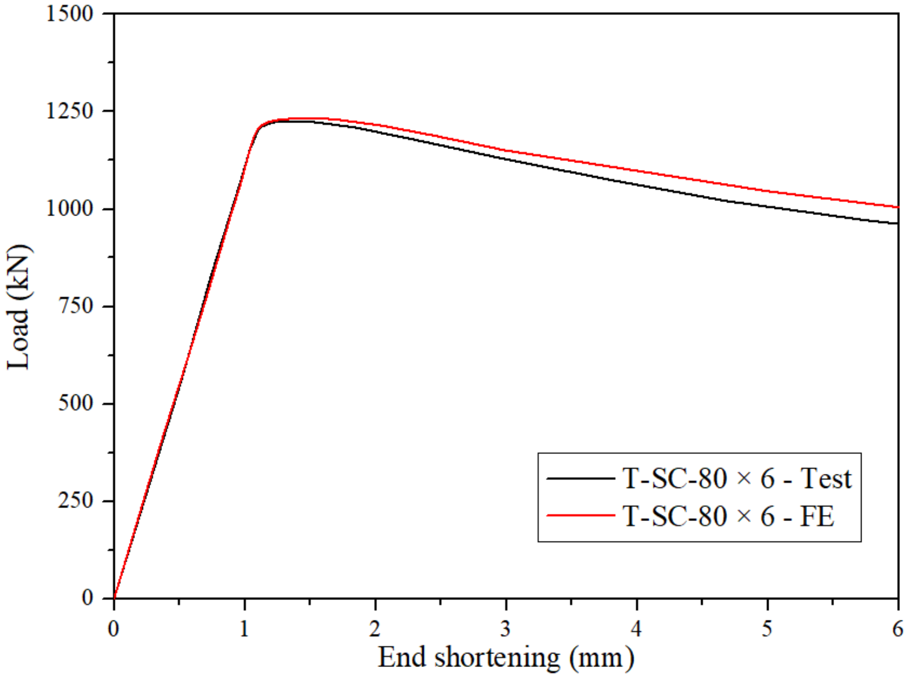

Fig. 16 Experimental and numerical load-end shortening responses of Q90 HSS welded T-section stub column T-SC-80 × 6

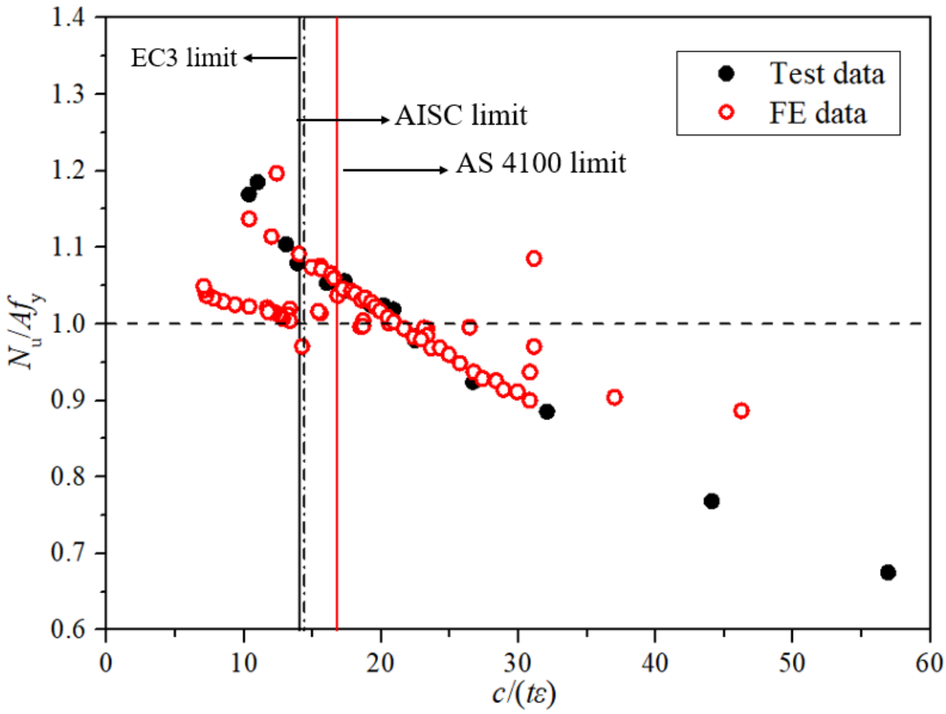

Fig. 17 Assessment of slenderness limit in design codes for outstand flanges of welded section in compression

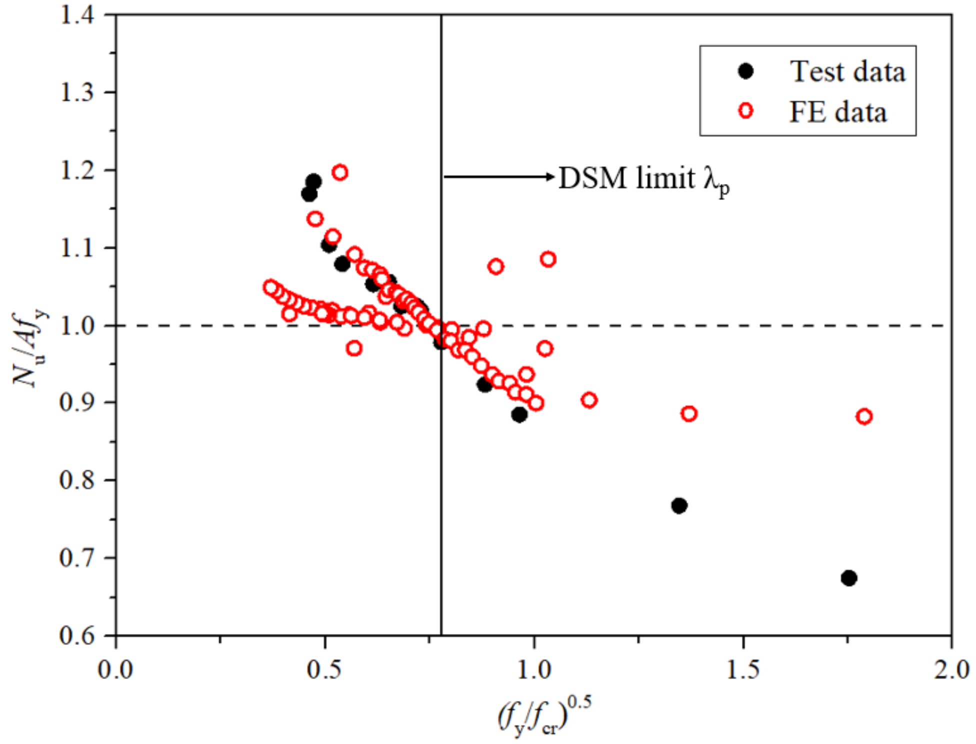

Fig. 18 Assessment of DSM cross section slenderness limit

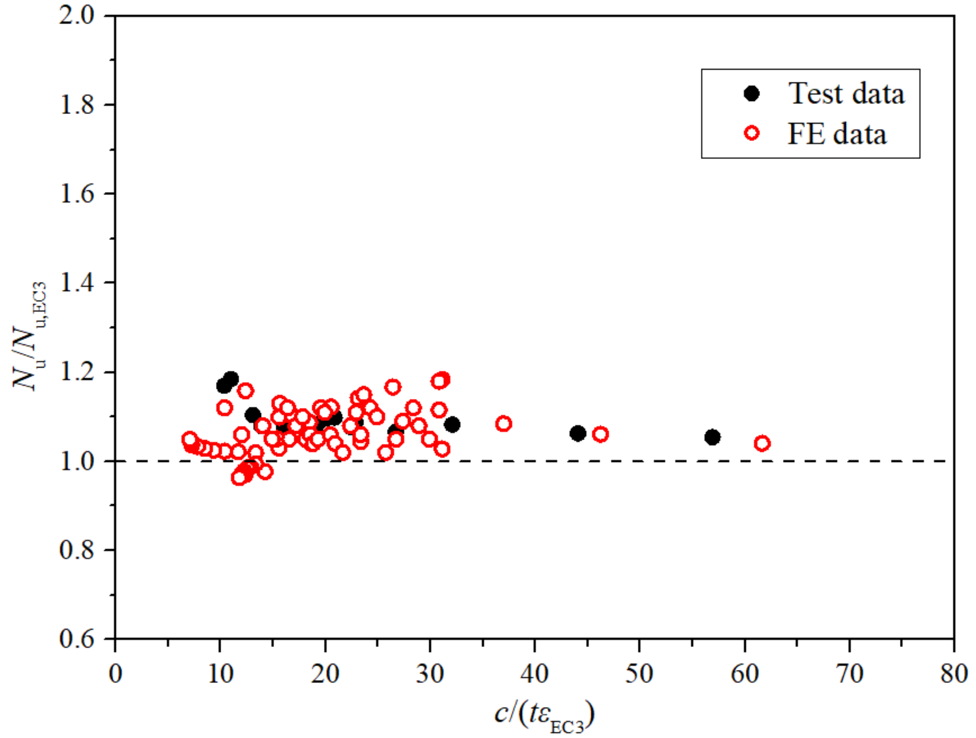

Fig. 19 Comparisons of experimental and numerical results with strength predictions from EC3

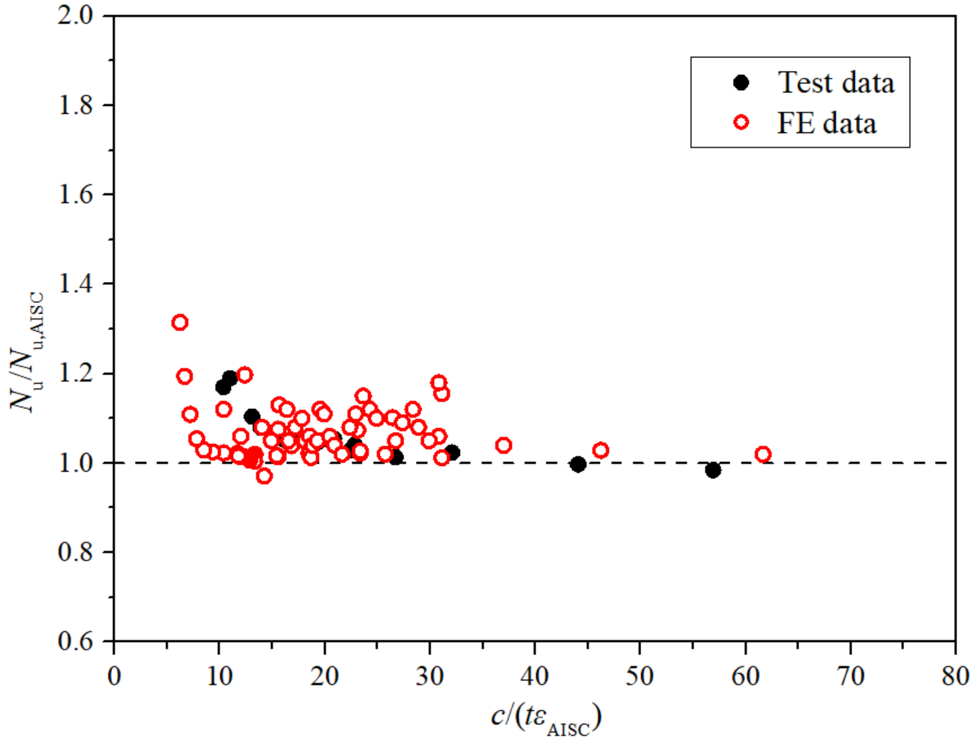

Fig. 20 Comparisons of experimental and numerical results with strength predictions from ANSI/AISC 360-16

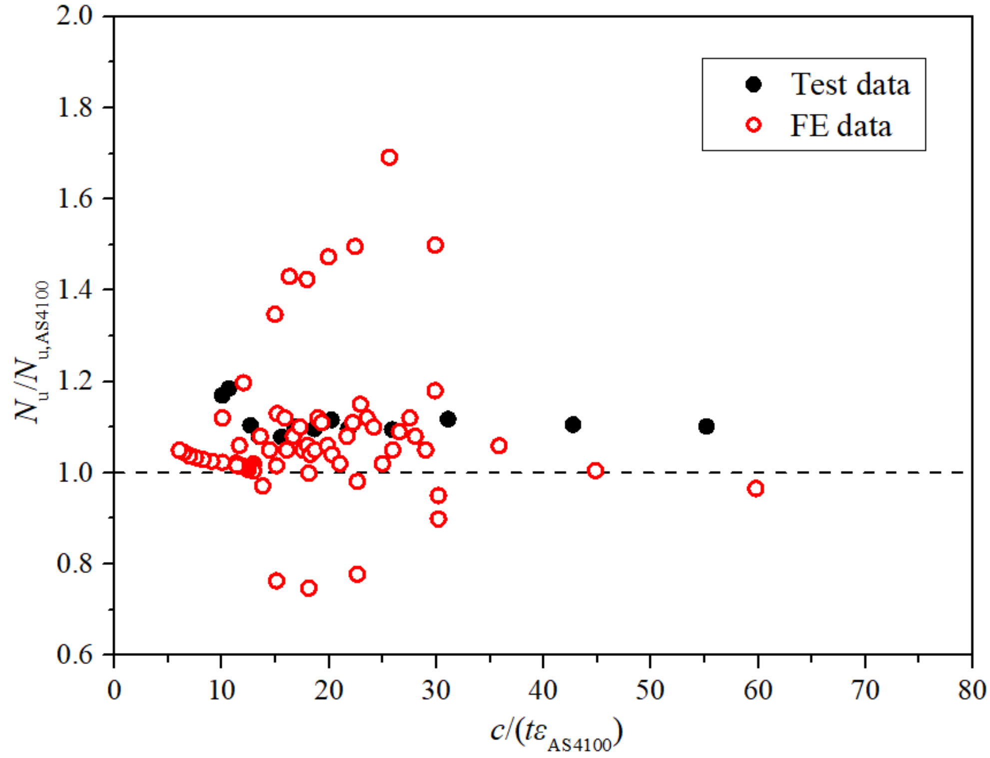

Fig. 21 Comparisons of experimental and numerical results with strength predictions from AS 4100

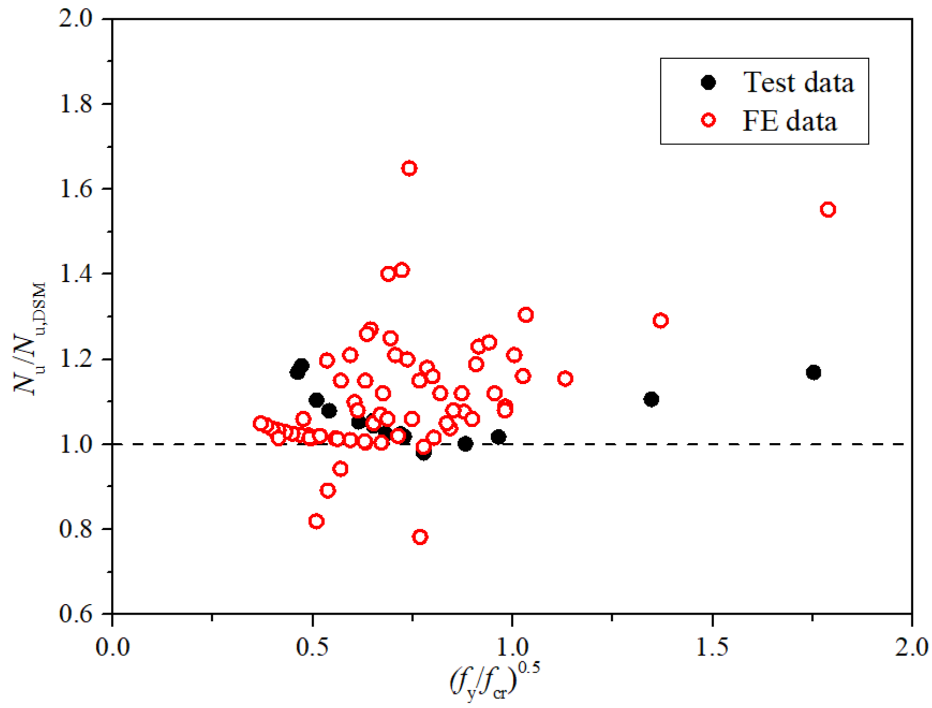

Fig. 22 Comparisons of experimental and numerical results with strength predictions from DSM

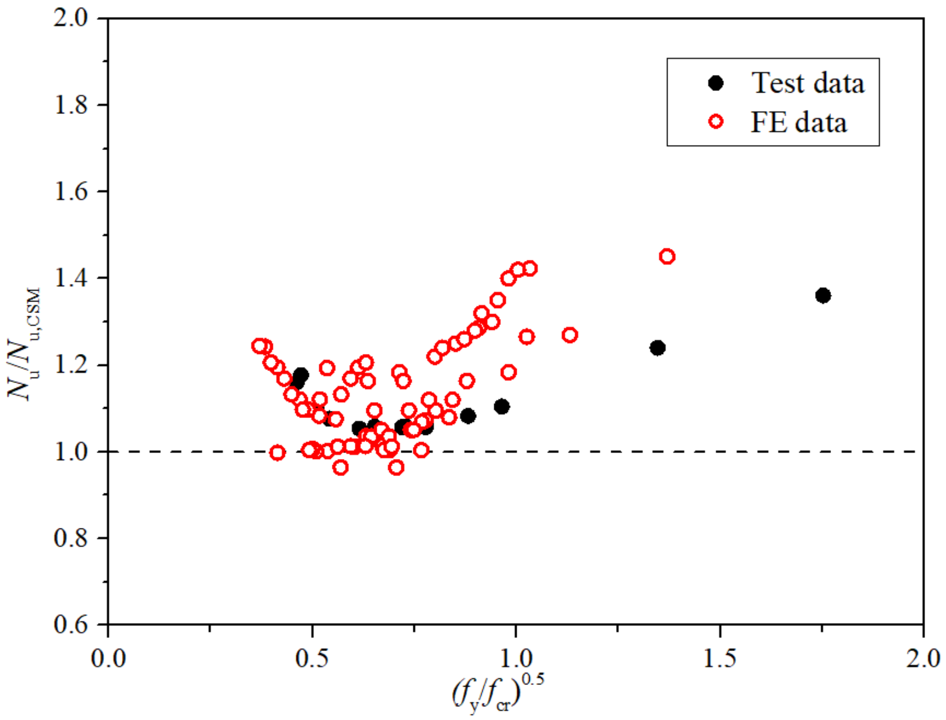

Fig. 23 Comparisons of experimental and numerical results with strength predictions from CSM

Table 1 Chemical compositions listed in mill certificates for 6 mm and 10 mm thick parent plates.

Steel plate	Chemical composition (wt%)										
	C	Mn	P	S	Si	Cr	Mo	Nb	Ti	B	CEV
6 mm plate	0.14	1.40	0.019	0.001	0.26	0.27	0.14	0.024	0.013	0.002	0.46
10 mm plate	0.14	1.40	0.019	0.001	0.27	0.26	0.15	0.024	0.013	0.002	0.46

Table 2 Chemical compositions of the welding electrode ER110S-G for Q690 steel plates.

Electrode	Chemical composition (wt%)										
	C	Mn	P	S	Si	Cr	Mo	Nb	Ti	V	Ni
ER110S-G	0.09	1.70	0.009	0.008	0.70	0.30	0.60	0.027	0.1	0.03	1.85

Table 3 Measured geometric dimensions and initial local geometric imperfections of HSS welded T-section stub column specimens.

Specimens	L (mm)	B (mm)	H (mm)	b_f (mm)	h_w (mm)	t_f (mm)	t_w (mm)	h_f (mm)	ω_0 (mm)
T-SC-55 × 6	200	110.1	54.6	43.0	35.9	9.63	6.35	9.07	0.08
T-SC-60 × 6	200	110.0	57.0	42.5	38.0	9.63	6.34	9.37	0.05
T-SC-65 × 6	200	110.0	64.5	42.4	45.3	9.64	6.35	9.56	0.08
T-SC-70 × 6	200	110.1	70.0	40.2	48.3	9.63	6.36	12.07	0.12
T-SC-75 × 6	250	110.2	73.5	43.8	55.7	9.65	6.36	8.15	0.18
T-SC-80 × 6	300	110.0	79.1	42.6	60.3	9.60	6.38	9.20	0.16
T-SC-80 × 6#	300	110.0	80.0	42.8	60.1	9.71	6.39	10.19	0.15
T-SC-85 × 6	300	109.9	83.5	44.7	66.7	9.70	6.36	7.10	0.21
T-SC-88 × 6	300	109.9	88.8	42.8	70.2	9.65	6.38	8.95	0.14
T-SC-90 × 6	300	109.9	90.0	44.3	72.8	9.70	6.39	7.50	0.11
T-SC-100 × 6	300	110.1	97.1	42.9	78.5	9.63	6.40	8.97	0.12
T-SC-100 × 6#	300	110.2	97.0	43.1	79.2	9.65	6.35	8.15	0.22
T-SC-110 × 6	350	110.1	111.9	42.9	93.3	9.66	6.40	8.94	0.18
T-SC-130 × 6	450	110.1	129.5	43.5	111.4	9.68	6.36	8.42	0.19
T-SC-170 × 6	550	110.2	169.2	46.0	153.6	9.64	6.38	5.96	0.26
T-SC-215 × 6	650	110.0	215.0	44.5	198.0	9.65	6.37	7.35	0.27

Note: # indicates a repeated test

Table 4 Measured material stress-strain curves from longitudinal and transverse coupon specimens from 6 mm thick parent plates.

Section	E_s (GPa)	f_y (MPa)	f_u (MPa)	ε_u (%)	ε_f (%)	ε_{sh} (%)
6 mm plate-L1	217.9	780	825	7.1	18.7	2.41
6 mm plate-L2	217.8	790	835	6.8	18.4	2.42
6 mm plate-L3	220.3	791	839	6.9	18.8	2.38
Mean	218.7	787	833	6.9	18.6	2.40
CoV	0.005	0.006	0.007	0.018	0.009	0.007
6 mm plate-T1	219.5	798	842	6.9	18.7	2.56
6 mm plate-T2	218.9	795	839	7.0	17.7	2.65
6 mm plate-T3	210.4	774	823	6.8	18.1	2.17
Mean	216.3	789	835	6.9	18.2	2.46
CoV	0.019	0.014	0.010	0.012	0.023	0.085

Table 5 Measured material stress-strain curves from longitudinal and transverse coupon specimens from 10 mm thick parent plates.

Section	E_s (GPa)	f_y (MPa)	f_u (MPa)	ε_u (%)	ε_f (%)	ε_{sh} (%)
10 mm plate-L1	214.8	812	839	6.8	18.7	3.48
10 mm plate-L2	213.9	818	846	6.8	18.4	3.48
10 mm plate-L3	219.5	815	844	6.5	18.2	3.61
Mean	216.1	815	843	6.7	18.4	3.52
CoV	0.011	0.003	0.003	0.021	0.011	0.017
10 mm plate-T1	219.0	824	853	6.9	17.8	3.49
10 mm plate-T2	216.8	817	845	6.3	18.4	3.45
10 mm plate-T3	216.3	817	847	7.0	18.8	3.31
Mean	217.4	819	848	6.7	18.3	3.42
CoV	0.005	0.004	0.004	0.046	0.022	0.023

Table 6 Summary of Q690 welded T-section stub column test results.

Specimens	$N_{u,test}$ (kN)	δ_u (mm)	$N_{u,test}/Af_y$	$N_{u,test}/N_{u,EC3}$	$N_{u,test}/N_{u,AISC}$	$N_{u,test}/N_{u,AS4100}$	$N_{u,test}/N_{u,DSM}$	$N_{u,test}/N_{u,CSM}$
T-SC-55 × 6	1276.2	4.38	1.17	1.17	1.17	1.17	1.17	1.16
T-SC-60 × 6	1306.0	4.64	1.19	1.19	1.19	1.19	1.19	1.18
T-SC-65 × 6	1259.5	4.12	1.10	1.10	1.10	1.10	1.10	1.10
T-SC-70 × 6	1261.4	3.83	1.08	1.08	1.08	1.07	1.08	1.08
T-SC-75 × 6	1252.2	2.98	1.05	1.08	1.05	1.08	1.05	1.05
T-SC-80 × 6	1280.2	2.83	1.06	1.09	1.06	1.10	1.06	1.06
T-SC-80 × 6#	1279.5	2.82	1.06	1.08	1.04	1.09	1.01	1.04
T-SC-85 × 6	1271.6	1.87	1.02	1.08	1.05	1.10	1.02	1.03
T-SC-88 × 6	1295.4	1.69	1.02	1.10	1.05	1.11	1.02	1.06
T-SC-90 × 6	1299.4	1.65	1.02	1.10	1.05	1.12	1.02	1.06
T-SC-100 × 6	1279.3	1.36	0.98	1.08	1.03	1.10	0.98	1.06
T-SC-100 × 6#	1288.5	1.42	0.97	1.09	1.04	1.11	0.99	1.07
T-SC-110 × 6	1279.4	1.85	0.92	1.07	1.01	1.09	1.00	1.08
T-SC-130 × 6	1302.9	2.02	0.89	1.08	1.02	1.12	1.02	1.10
T-SC-170 × 6	1283.4	2.53	0.77	1.06	0.99	1.11	1.11	1.24
T-SC-215 × 6	1281.1	2.84	0.67	1.05	0.98	1.10	1.17	1.36
			Mean	1.08	1.06	1.11	1.06	1.11
			CoV	0.018	0.05	0.012	0.059	0.077

. Note: # indicates a repeated test

Table 7 Comparison of the stub column test results with finite element results for various imperfection amplitudes.

Specimens	$N_{u,FE}/N_{u,test}$			
	ω_0	$t_w/10$	$t_w/50$	$t_w/100$
T-SC-55 × 6	0.99	0.98	0.99	0.99
T-SC-60 × 6	1.03	1.00	1.02	1.03
T-SC-65 × 6	1.03	1.01	1.02	1.03
T-SC-70 × 6	1.04	1.02	1.03	1.04
T-SC-75 × 6	1.03	1.01	1.02	1.03
T-SC-80 × 6	0.99	0.97	0.98	0.99
T-SC-80 × 6#	0.99	0.97	0.98	0.99
T-SC-85 × 6	1.00	0.98	0.99	1.00
T-SC-88 × 6	1.01	0.99	1.00	1.01
T-SC-90 × 6	1.01	1.00	1.01	1.02
T-SC-100 × 6	1.02	1.01	1.02	1.03
T-SC-100 × 6#	1.02	1.01	1.02	1.03
T-SC-110 × 6	1.01	0.99	1.01	1.01
T-SC-130 × 6	1.03	1.04	1.05	1.06
T-SC-170 × 6	1.04	1.05	1.06	1.07
T-SC-215 × 6	1.05	1.07	1.08	1.09
Mean	1.02	1.01	1.02	1.03
CoV	0.02	0.03	0.03	0.03

Note: # indicates a repeated test

Table 8 Summary of EC3, AISC, AS, DSM and CSM slenderness limits between slender and non-slender plate elements in compression.

Design standards and methods	Yield slenderness limits
EN 1993-1-12	$c/t \leqslant 14\varepsilon_{EC3}$
ANSI/AISC 360-16	$c/t \leqslant 0.64\varepsilon_{AISC}$
AS 4100	$c/t \leqslant 14\varepsilon_{AS4100}$
DSM	$\lambda_p = 0.776$
CSM	$\lambda_p = 0.68$

Table 9 Comparisons of test and FE results with predicted strengths.

Number of Specimen		$N_u/N_{u,EC3}$	$N_u/N_{u,AISC}$	$N_u/N_{u,AS4100}$	$N_u/N_{u,DSM}$	$N_u/N_{u,CSM}$
Test:16	FE:88					
	Mean	1.06	1.05	1.09	1.08	1.12
	CoV	0.05	0.06	0.15	0.14	0.13
	b	1.05	1.08	1.05	1.04	1.08
	V_δ	0.05	0.06	0.22	0.12	0.11
	V_r	0.09	0.09	0.17	0.14	0.14
	γ_{M0}	1.16	1.15	1.32	1.27	1.24
	γ_{M0}^*	1.04	1.03	1.18	1.13	1.11